Brigham Young University
BYU ScholarsArchive

All Theses and Dissertations

2012-06-08

Evaluation of Advanced Conductive Nickel Materials for Strain Sensing in Carbon Fiber Reinforced Polymers

Michael Christian Koecher
Brigham Young University - Provo

Follow this and additional works at: https://scholarsarchive.byu.edu/etd

 Part of the Mechanical Engineering Commons

BYU ScholarsArchive Citation

Koecher, Michael Christian, "Evaluation of Advanced Conductive Nickel Materials for Strain Sensing in Carbon Fiber Reinforced Polymers" (2012). *All Theses and Dissertations*. 3580.
https://scholarsarchive.byu.edu/etd/3580

This Thesis is brought to you for free and open access by BYU ScholarsArchive. It has been accepted for inclusion in All Theses and Dissertations by an authorized administrator of BYU ScholarsArchive. For more information, please contact scholarsarchive@byu.edu, ellen_amatangelo@byu.edu.

Evaluation of Advanced Conductive Nickel Materials for Strain Sensing in Carbon Fiber Reinforced Polymers

Michael Christian Koecher

A thesis submitted to the faculty of
Brigham Young University
in partial fulfillment of the requirements for the degree of

Master of Science

David T. Fullwood, Chair
Anton E. Bowden
Mark B. Colton

Department of Mechanical Engineering
Brigham Young University
June 2012

Copyright © 2012 Michael Koecher
All Rights Reserved

ABSTRACT

Evaluation of Advanced Conductive Nickel Materials for Strain Sensing in Carbon Fiber Reinforced Polymers

Michael Koecher
Department of Mechanical Engineering, BYU
Master of Science

Due to their unique properties, carbon fiber reinforced polymers (CFRP) are becoming ever more prevalent in today's society. Unfortunately, CFRP suffer from a wide range of failure modes and structural health monitoring methods are currently insufficient to predict these failures. It is apparent that self-sensing structural health monitoring could be advantageous to protect consumers from catastrophic failure in CFRP structures. Previous research has shown that embedded nickel nanostrand nanocomposites can be used to instantaneously measure strain in carbon fiber composites, but these methods have been severely limited and can induce high stress concentrations that compromise the structural integrity of the carbon fiber structure. In this research the strain sensor material and the connective circuitry to the sensor are analyzed to improve the practicality of in situ strain sensing of carbon fiber structures. It has been found that the use of nickel nanostrands embedded directly onto carbon fiber as a strain sensor material has no advantages over a carbon fiber strain sensor alone. Additionally, it has been shown that the circuitry to the strain sensor plays a critical role in obtaining a strong, consistent piezoresistive signal that can be related to strain. The use of nickel coated carbon fiber in the circuitry has been evaluated and shown to reduce the noise in a piezoresistive signal while allowing for remote strain sensing from greater distances away from the strain location.

The piezoresistive strain sensing utilized in the tested sensor designs relies on electrons tunneling through an insulting barrier between two conductors. This phenomenon is known as quantum tunneling. Two factors - tunneling barrier height and gap distance - affect the probability of quantum tunneling occurring. Thus, to accurately model and predict the piezoresistivity of nanocomposites these two parameters must be known. Through the use of dielectric spectroscopy the gap distance can be determined. Using nanoindenting, the barrier height for various polymers was also determined. The measured values can be used, in future work, to improve the modeling of nickel nanostrand nanocomposite.

Keywords: carbon fiber, nanocomposite, nickel nanostrands, strain sensing, barrier height

ACKNOWLEDGEMENTS

There are many that without their help this research would not be possible. First, I would like to thank Dr. David Fullwood for the all the advice, encouragement, and direction given during this research. A dditionally, I would like to thank my committee Dr. Colton, and Dr. Bowden. A special thanks Nathan Hansen from Conductive Composites Company for all the materials he provided, John Yeager from Los Alamos National Labs for his time and efforts, and Dr. John Colton and Tyler Park from the BYU physics department for helping me understand and measure dielectric samples. Finally, without the diligence of my undergraduate research assistants John Pande, Scott Merkley, and Sam Henderson this research would have been severely delayed. Thank you all.

TABLE OF CONTENTS

LIST OF TABLES

LIST OF FIGURES

1 INTRODUCTION

1.1 Carbon Fiber Composites

When designing a product there are generally four classes of materials that can be chosen from: metals, ceramics, polymers or composites [1]. Composite materials form a field of particular interest that combines at least two differing materials; one is often considered the reinforcement and the other is the matrix. This combination of different materials potentially creates a new material that has beneficial properties from both constituents that cannot be seen in each material individually [2]. One such subclass of composites that is growing ever more popular is carbon fiber reinforced polymer composites (CFRP).

Carbon fiber composites are becoming increasingly prevalent in products throughout the world. In fact, it is estimated that by 2014 global sales of CFRPs will increase to $28 billion, an 87% increase from 2008 [3]. This remarkable increase is due to the fact that CFRP have the advantages of high strength-to-weight ratio, low thermal expansion, and good fatigue resistance [4]. Also, carbon fiber composites laminas are highly anisotropic meaning that one can orient strength into the design were it is needed while limiting the excess material, weight, and strength in directions of insignificant loading [5].

One of the main disadvantages of CFRPs structures is that it is difficult to determine internal structural damages [1, 4]. Many of the methods to determine loading and internal damage require that the structure be analyzed in a lab, most often when the product has

been taken out of service. T his seems insufficient when the product being considered is something like a wing on a passenger airplane. It would be advantageous to have a way to instantaneously measure the strain while a product is in service. Not only would this increase the safety for consumers of a CFRP product but it also could be used to retrieve useful information such as the impact of a golf ball on a carbon fiber shaft, the impact a rider has on a carbon fiber snowboard, or the stresses induced on a windmill blade during high winds.

Countless hours of research have been done to determine a variety of methods of strain sensing in a CFRP. Each method is coupled with its own advantages and disadvantages. Recent research at BYU has concluded that a novel use of nickel nanostrands (NiNs) can be used as in situ strain sensors in a carbon fiber structure [6]. Being in its infant stage there are many hurdles that make these NiN sensors more of a theoretical, rather than practical, solution. In this research tests are performed to expand upon these developments and create a practical embedded strain sensor. New methods in patch placement, measurement techniques, and fiber orientation are used to evaluate the benefits, if any, of nickel nanostrands as in situ strain sensors in carbon fiber layups composed of multidirectional fibers and compare these with standard piezoresistive behavior of neat carbon fiber structures.

1.2 Nanocomposite Modeling Parameters

Production and characterization of nanocomposites are growing fields of interest due to the advantageous material properties obtained when nano-scale particles are combined with a bulk material [7]. Important material properties such as electrical conductivity can be modified by using nanoparticles or nano-sized wires [8-10]. These specialized conductive nanocomposites are finding many applications in industry such as EMI shielding [11], flexible circuits[12], and high fatigue life electrodes for biomedical applications [12]. One of the most promising aspects

of conductive nanocomposites is using the piezoresistivity that they exhibit to measure strain in a material [12-14].

Common conductive fillers used in these nanocomposites are carbon nanotubes [15], carbon black [16], and nickel nanostrands [17]. Immense amounts of research have focused solely on carbon nanotubes and carbon black. Nickel nanostrand research is a more recent development and has shown to be a more conductive filler in a nanocomposite [18].

To better understand the piezoresistivity of the nanocomposite the conductivity should first be examined. The conductivity of these nanocomposites is commonly modeled using percolation theory in conjunction with quantum tunneling. Two parameters in particular, quantum tunneling barrier height and adsorbed layer thickness have been examined for various polymers used in conductive nickel nanostrand nanocomposites. Two previously reported techniques, nanoindentation and dielectric spectroscopy, will be combined to provide insights into the physical properties of conductive nano-composites in order to understand their unique piezoresistive properties. Nanoindention records voltage and depth of a tip pressed into a polymer to measure the barrier height while dielectric specstroscopy uses the relaxation characteristics at high frequencies to determine the junction distance between nanostrands which is then correlated to the adsorbed layer thickness.

Chapter 2 addresses strain sensing in multidirectional carbon fiber laminates while Chapter 3 evaluates the use of nanoindentation and dielectric spectroscopy to calculate quantum tunneling barrier height and junction gap distances.

2 STRAIN SENSING IN CARBON FIBER COMPOSITES

2.1 Current Strain Sensing Methods

Strain sensing in CFRP has been extensively researched, resulting in various methods of measuring strain in carbon fiber structures. Each method has its own set of advantages, along with corresponding drawbacks, often preventing use over a wide set of applications. Such methods include: traditional foil strain gauges, fiber Bragg grating, Raman wavenumber sensing, and piezoresistive self-sensing.

2.1.1 Traditional Foil Strain Gauges

Traditional strain gauges are composed of thin metal films that change resistance when strained. These gauges are simply glued to the surface of the structure in which strain is to be measured [19]. The advantages of these types of gauges are that they are fairly simple to install, low cost, and have proved to be successful through years of use in industry. Because these gauges are simply adhered to the surface they are susceptible to damage, can easily fall off and are poor in high strain applications. Furthermore, wires must be routed across or though the structure to carry the required signal to the monitoring unit.

2.1.2 Fiber Bragg Grating

Fiber Bragg grating uses fiber optics and light transmission to measure strain [20]. A grating in the fiber manipulates the laser light as it passes through it. As the fiber is strained the grating is altered thus the laser light is altered as well which can be correlated to strain. This is a complex method that can be used in carbon fiber structures for in situ strain sensing but the cost can be prohibitive [17].

2.1.3 Raman Wavenumber Sensing

Raman wavenumber sensing is a very valuable technique that shines a laser onto the surface and detects the wavelength and intensities of the light that is reflected to determine strain, stress concentrations, and micro-failures [21]. While this gives valuable, accurate information it is infeasible for in situ strain sensing in typical environments.

2.1.4 Piezoresistive Self-Sensing Carbon Fiber

It has been shown that carbon fiber itself is piezoresistive in nature [22]. Thus it is possible to measure a resistance change in a carbon fiber structure when strained [23, 24]. This would be an ideal solution but is limited in its capability as will be discussed below. It will be seen that with the use of embedded nickel coated carbon fiber that the feasibility of using the piezoresistive nature of carbon fiber as a strain sensing material is expanded.

2.1.5 Nanocomposite Strain Sensing

Research has shown that piezoresistive nanocomposites can provide an alternative method for measuring strain. A nanocomposite is a material that is composed of two or more phases with one phase being a nano-scale filler material. Examples of conductive nano-fillers

that have been used in strain sensors include carbon nanotubes [15], carbon black [16], and nickel nanostrands [17].

Strain sensors made of nanocomposites appear to operate in the same way as a traditional metal foil strain gauge; as the sensor is strained there is a piezoresistive change in the sensor which can be read and correlated with a percent strain. However, the physical phenomenon behind the resistance change in the gauge is fundamentally different. As a foil gauge is strained, the conductor length is increased and the cross section decreases, leading to higher resistance. In a nanocomposite a conductive network is provided by a conductive nano-filler within what is typically an insulating bulk material. As the material is strained the volume fraction, alignment and gaps between conductive nano-strands can change. We will focus on the evolution of these gaps, which can lead to the most radical resistance change. This phenomenon has been modeled using quantum tunneling and percolation theory and is discussed further in Chapter 3.

The change in number of conductive nanojunctions causes a piezoresistive effect in the bulk properties of the nanocomposite [25]. This makes conductive nanocomposites a viable option for strain sensing in a CFRP.

2.1.6 Nickel Nanostrand Nanocomposites

As mentioned previously multiple nano-fillers exist which could be used for strain sensing in carbon fiber structures. Previous research by Johnson et al. has shown different methods of using nickel nanostrands as strain sensors in carbon fiber structures [17]. One method involves making a nickel nanostrand nanocomposite patch, insulating it, and inserting it into a carbon fiber structure. This method worked well, in that it was able to measure strain as well as detect damage to the structure. Unfortunately, inserting such a large patch with wire

leads dramatically increases the number of stress concentrations and, consequentially, weakens the carbon fiber structure.

Another method developed by Johnson was to directly embed a patch of nickel nanostrands between layers of carbon fiber prepreg. This proved to be effective for measuring strain when using unidirectional fibers. Once multidirectional layups were used no appreciable strain reading was detected. In this research directly embedding nickel nanostrands into a multidirectional carbon fiber laminate are compared to samples in which no embedded nanostrands are used.

2.2 Objective

As mentioned previously current methods for instantaneously measuring strain in a carbon fiber composite are lacking. The introduction of nickel nanostrand nanocomposites into carbon fiber structures has been shown to measure strain in carbon fiber structures as well as allow for remote sensing of a strain location. Yet this method is inadequate due to the adverse effects on the strength of the structure. Additionally, without creating a relatively large insulated nanocomposite patch a piezoresistive signal was deemed unobtainable from multidirectional laminates.

The objective of this research is to explore the use of advanced conductive nickel materials (nickel nanostrands and nickel coated carbon fiber) for in situ strain sensing in multidirectional carbon fiber laminates without significantly reducing the strength of the carbon fiber component. Also, it is desired that the method employed to measure the piezoresistive signal does not require extra steps in the manufacturing processes (such as developing an insulted patch), but more closely mimics the simplified process of directly embedding nickel nanostrands as implemented by Johnson.

To accomplish this, two variables were considered: the piezoresistive sensor and the circuitry that connects the sensor to a resistance meter. In this research two piezoresistive sensor types were considered: 1) the carbon fiber prepreg of the structure and 2) the carbon fiber of the structure embedded with nickel nanostrands.

In this research, methods are explored for sensing strain at a remote location from the resistance monitoring systems. Thus, in terms of this research the word circuitry refers to the conductive path between the piezoresistive sensor and the resistance measuring probes from the resistance meter. This circuitry is examined by altering resistance probing locations as well as the material used for the circuitry path. The use of highly conductive nickel coated carbon fiber versus carbon fiber prepreg is compared to determine what kind of circuitry is most advantageous.

2.3 Experimentation

2.3.1 Materials

Along with traditional fiber-reinforced polymer materials, two additional components were used in the construction of the strain sensing sensors and circuits. Nickel nanostrands (NiNs) are a highly conductive nickel structure on the nanoscale. The high strand aspect ratio and the bifurcated structure allow conductivity to be obtained at small volume fractions of nanostrands [26]. An SEM image of the complex NiN structure taken by the author can be seen in Figure 2-1. It is evident from Figure 2-1 that there is a wide range of individual nanostrand sizes.

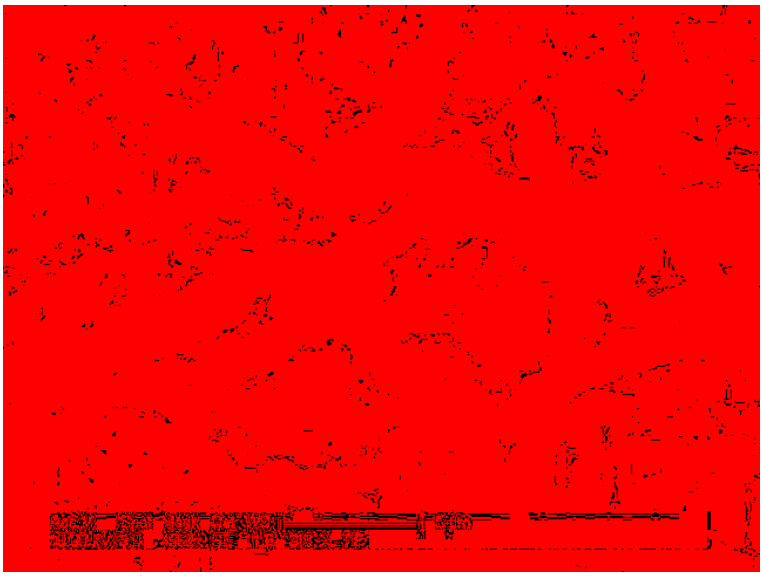

Figure 2-1: SEM image of nickel nanostrands.

The other novel material reported in this paper, as the basis for sensor circuitry, is nickel coated carbon fiber (NCCF); this is carbon fiber that has a uniform coating of nickel applied to its surface through a chemical vapor deposition process. These coated fibers are much more conductive than bare carbon fiber and are often used to aid in electrical shielding in carbon fiber structures [27]. An SEM image of nickel coated carbon fiber can be seen in Figure 2-2. Both the nickel nanostrands and the nickel coated carbon fiber were produced and provided by Conductive Composites Company (Heber, Utah). The more traditional carbon fiber composite used in this research is a unidirectional carbon fiber prepreg ZR6-P35, provided by Zoltek. A SP3817781 OST type plain fabric weave fiberglass prepreg was also used.

Figure 2-2: SEM images of nickel coated carbon fiber (image provided courtesy of Nathan Hansen, Conductive Composites Company)

2.3.2 Sample Preparation

Components with various pre-preg layups were created to determine the capability and limitations of the embedded conductive materials for in situ strain sensing. For initial sensor evaluation, laminates were formed suitable for tensile testing. Each carbon fiber laminate was composed of layers of prepreg cut to 250 mm x 25 mm. Woven fiber glass tabs were adhered to the ends of the carbon fiber samples to insulate the sample from the metal grips of the tensile tester and ensure that these did not interfere with the signal. Also, the fiberglass tabs prevented the metal grips from penetrating and damaging the underlying carbon fiber.

Each sample consisted of a patch location and a patch material. The patch location refers to the area that strain is to be measured and the patch material was either prepreg embedded with NiNs or the carbon fiber prepreg itself. To limit variation and guarantee uniformity in the samples with embedded nanostrands, 0.02 g of nickel nanostrands were filtered through a 60 mesh screen (250 μm) before being placed in a patch area of 19 mm by 12 mm. Research by Johnson showed that 0.02 g of NiN embedded in carbon fiber was the optimal amount to create a piezoresistive percolating network [6]. For carbon fiber and NiN patches the [0] direction

(prepreg oriented parallel to the applied strain) and [90] direction (prepreg oriented transverse to the applied strain) were evaluated as the sample was strained in the direction of its length.

In the research conducted by Johnson samples were created by laying up four layers of unidirectional prepreg, nanostrands were spread in a small area, and four more layers of prepreg on top (see Figure 2-3). Probing of the sample occurred some distance away from the patch location but wires were not needed because the conductive nature of the carbon fiber acted as conductive leads to the patch. The complete layup was then cured in an autoclave to the prepreg manufactures specifications. This method proved successful for unidirectional layups but when multidirectional layups were used the cross directional fibers would short-circuit the carbon fiber leads and eliminated the current flow through the piezoresistive patch.

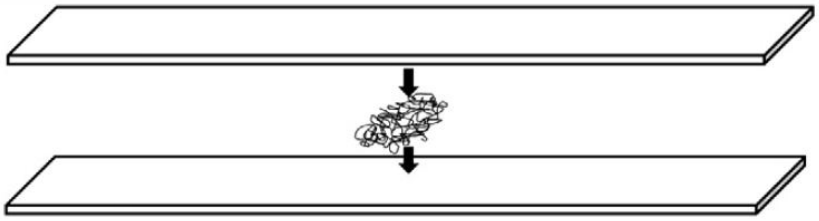

Figure 2-3: Layup method conducted by Johnson (courtesy of Johnson)

In the current work, the configuration was modified to enable the embedded patch concept to work for multidirectional layups; to do this the patch needed to be located where it was only in contact with carbon fibers aligned in a single direction. This was accomplished by moving the patch from the center of the carbon fiber structure to the outer layer of carbon fiber. The patch of nickel nanostrands was then covered with a small piece of carbon fiber prepreg to prevent movement of the nanostrands while curing and to protect the nanostrand patch while the structure was in service. In theory, the current from the input probe will flow into the carbon

fibers in the [0] orientation and down through the NiNs and back into the carbon fibers leading to the output probe. For this layup to be successful, the current must only follow the described path and not short circuit. Figure 2-4 illustrates the new layup method described above. Similar samples were made with varying fiber orientations with and without embedded nickel coated carbon fiber. Also, the placement of the probes and the nickel coated carbon fiber where altered as will be discussed below.

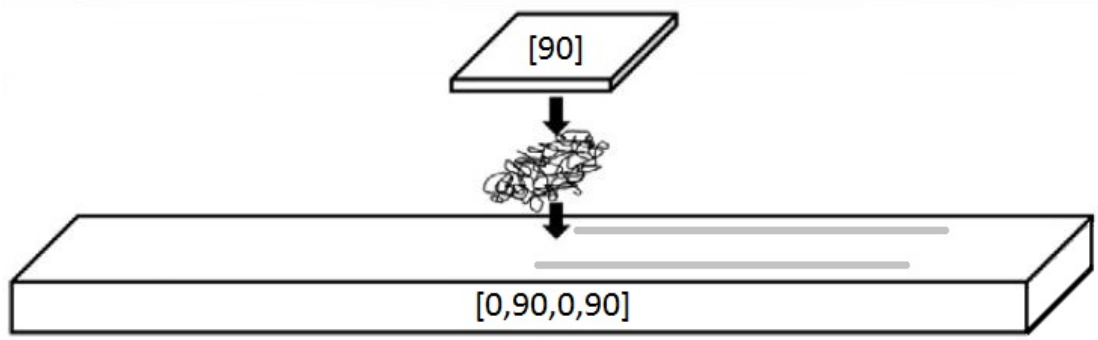

Figure 2-4: Example of new NiN patch location in a multidirectional layup with NCCF (grey lines).

As is suggested by the name, nickel coated carbon fibers are carbon fibers that have been coated with nickel through a chemical vapor deposition process. These coated fibers are at least three times more conductive than bare carbon fiber [28].

One issue when using carbon fiber as a pseudo-wire to the nanostrand patch is that the carbon fiber wires are not insulated from each other. The only thing controlling the path of the electricity is the fact that carbon fiber is much more conductive in the longitudinal direction as opposed to the transverse direction. In the longitudinal direction the current travels along the carbon fiber and does not have to tunnel from fiber to fiber across the insulating matrix as it must in the transverse direction. If the probing occurs further and further away from the patch

location the greater the influence of the resistance in the carbon fibers compared to the patch location, and the noisier the signal becomes.

Using higher conductivity NCCF rather than uncoated carbon fibers as pseudo-wire leads helps control the flow of current. Since electricity flows in the path of least resistance most of the current is going to travel in the route of the NCCF. It was hypothesized that with the use of NCCF a better signal can be obtained at further distances compared with plain carbon fiber. Thus tests were performed with nickel coated carbon fiber leads as the connective circuitry from the piezoresistive patch to the resistance meter and compared to samples that used carbon fiber prepreg as the connective circuitry.

2.3.3 Test Method

The four probe resistance measurement method was used to measure the piezoresistive signal because it is a common method to eliminate contact resistance readings when contact resistance is significant as compared to the resistance of the component [29]. In this method a known current is passed through the outer probes and a voltage is read between the inner probes. Since no current is passing through the inner probes there is no contact resistance. A National Instruments NI 9219 multifunctional module was set to four probe resistance readings for these tests. A constant current of 500 μA was applied to the outer probes while a voltage was read across the inner probes. Using ohms law an output of resistance was obtained.

Three different configurations of probing to measure the piezoresistive change at the patch location were evaluated in this research. In the first method, referred to as the "collinear" probing method, four collinear probes were placed on the carbon fiber sample to eliminate contact resistance. For the second method the probes were placed in a "box" configuration. The box configuration is similar to the collinear method except there are two pseudo-wires instead of

four and each wire has two probes on it. In the final method, referred to as "longitudinal" probe method, the probes were place on each side of the patch. In each method the pseudo-wires consist of either the conductive carbon fiber prepreg or the embedded NCCF. Figure 2-5 depicts the difference between the three probing methods.

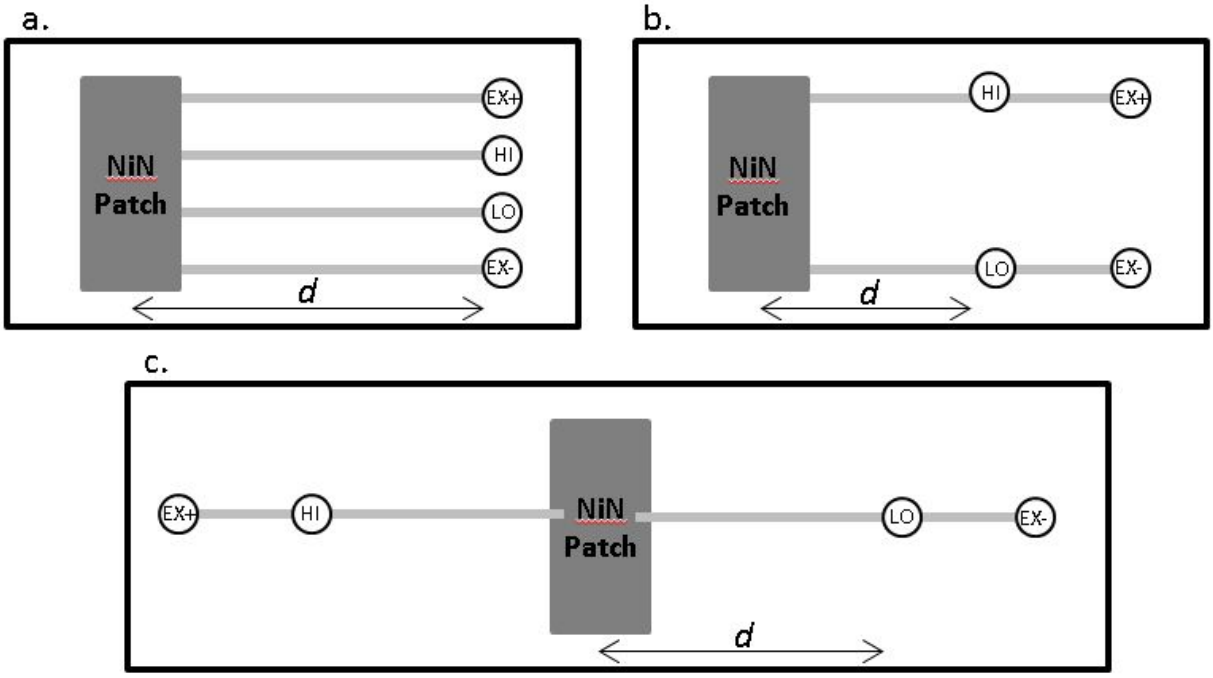

Figure 2-5: (a) Transverse collinear probe method, (b) Box probe method, and (c) Longitudinal probe method. In each method the grey lines represent the circuit path using either the carbon fiber strands from the structure or embedded NCCF. EX+ and EX- are the input and output current probes while HI and LO are the voltage reading probes.

In order to ensure consistent spacing and depth of the probes, transparent plastic plates, with an array of holes, were made to allow for rearrangement of the probes for each probing method, as can be seen in Figure 2-6 for each probing method. Note that in Figure 2-6 the photograph of the longitudinal method only shows two of the four probes.

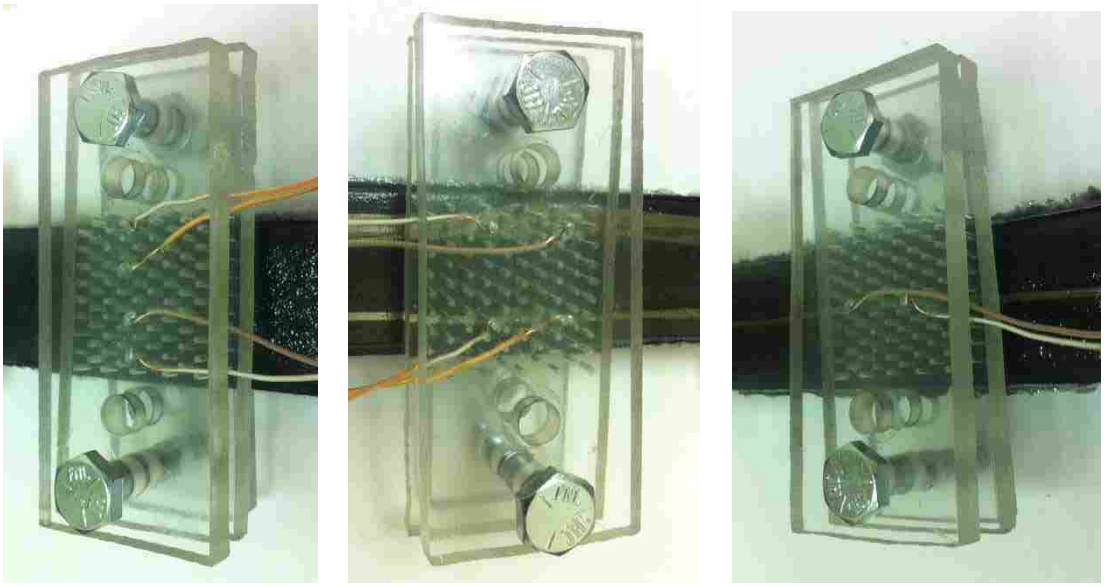

Figure 2-6: Pictures of actual probing using Collinear, Box, and Longitudinal methods, respectively.

Samples were cyclically loaded in tension in an Instron tensile tester to a prescribed strain of 0.30 % at a rate of 0.1 Hz in order to determine the feasibility of each configuration as in situ strain sensing for multidirectional carbon fiber laminates. Three point bending tests were also performed on select samples using supports 12.5 cm apart with a 10 mm vertical displacement of the wedge to determine the piezoresistive changes due to tension and compression. During loading the resistance measurements were sampled at a rate of 100 Hz and a moving average of 10 was used to improve signal smoothness.

To quantitatively evaluate the piezoresistive signal that was obtained a metric needed to be used. Sirohi and Chopra claim that piezoelectric strain sensors have superior performance in terms of signal-to-noise ratio (SNR) as compared to foil strain gauges [30]. To compare the resistive strain measurements a SNR value was calculated for each set of experimental data. This was calculated by first filtering the raw data using a fifth order Butterworth low-pass filter which was set to eliminate frequencies above 0.2 Hz which is above the known test straining

frequency of 0.1 Hz. Figure 2-7 shows the raw data, filtered signal, and the remaining noise. The root-mean-squared amplitude of the filtered signal was compared to the root-mean-squared amplitude of the noise in the SNR calculation as given by:

$$SNR = \left(\frac{A_{rms_{signal}}}{A_{rms_{noise}}}\right)^2 \tag{2-1}$$

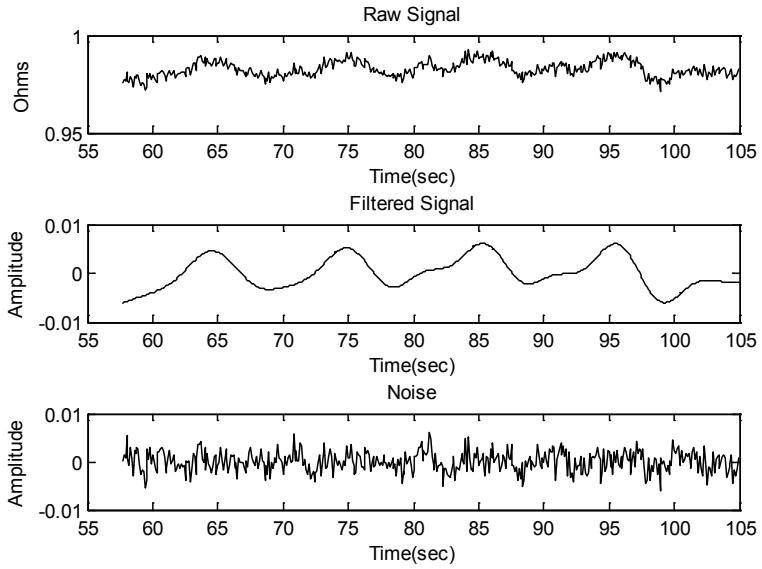

Figure 2-7: A signal (top) decomposed into a filtered signal (middle) and noise signal (bottom).

The signal-to-noise ratio (SNR) was calculated and used as a metric in the laboratory to quantitatively compare the piezoresistive signal between samples. A larger SNR correlated to a higher quality piezoresistive signal. In general, it was observed that a SNR value lower than about 0.30 suggested that there is no distinguishable signal that can be correlated to strain; an ideal SNR for non-laboratory situations has not been determined.

2.4 Results and Discussion

2.4.1 Nickel Coated Carbon Fiber

To determine the feasibility of using NCCF as pseudo-wires to the piezoresistive patch it was first necessary to determine if piezoresistive properties exist in NCCF. If the NCCF display a piezoresistive response, this will confuse the signal expected from the sensor. Tensile tests were performed on carbon fiber and NCCF and compared in Figure 2-8. It can be seen that the NCCF is much more conductive than carbon fiber and does not exhibit piezoresistive properties. This suggested that using NCCF as pseudo-wires to the patch does not contribute to the piezoresistive signal, and one can be confident that the strain being measured is precisely located at the patch location.

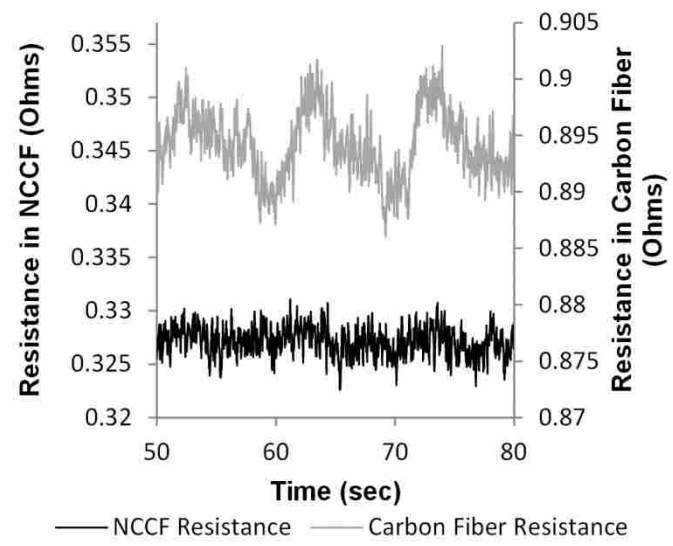

Figure 2-8: Comparison of the piezoresistivity of carbon fiber to the more conductive NCCF.

2.4.2 Collinear Probing

Collinear probing on a sample with a NiN patch embedded in the middle of a multidirectional layup shows no appreciable piezoresistive signal as shown by Johnson [17]. In

this scenario the cross-directional (90°) carbon fibers allow the current to flow directly between the current input and output probes and not through the piezoresistive NiN patch.

To try and alleviate this problem the patch was moved to the top layer of a multidirectional layup where the carbon fiber was oriented in the [0] direction as is shown in Figure 2-4. The layups tested consisted of four layers in the following pattern [90, 0, 90, 0] with and without a NiN patch on the outer [0] layer. Regardless of the patch when measuring the resistance using the collinear method illustrated in Figure 2-5a there was no piezoresistivity in the resulting signal. Figure 2-9 shows a typical result for this type of orientation.

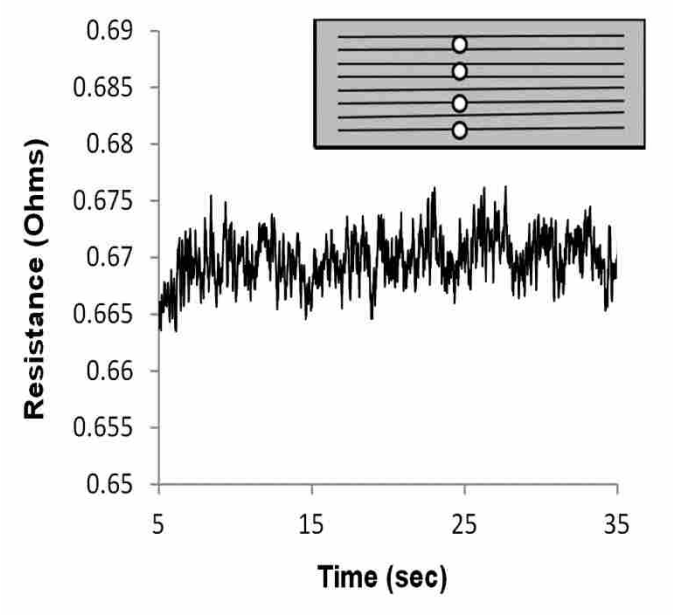

Figure 2-9: Collinear probing with probes placed perpendicular to the carbon fiber direction on the surface.

When the collinear probes were rotated and oriented parallel to the fibers on the outer layer a piezoresistive signal was obtained (see Figure 2-10). This result was typical regardless of having a NiN patch embedded on the surface. This signal can be attributed to the piezoresistivity of the carbon fiber itself. Thus carbon fiber alone can be used to measure strain in a

multidirectional layup if the distance between probes is sufficiently small. Tests were conducted using NCCF with this probing configuration but the tests consistently yielded no results thus eliminating the option of remote probing with this method. Using the box method and the longitudinal method in conjunction with NCCF it can be seen that remote probing at a very specific patch location can be obtained.

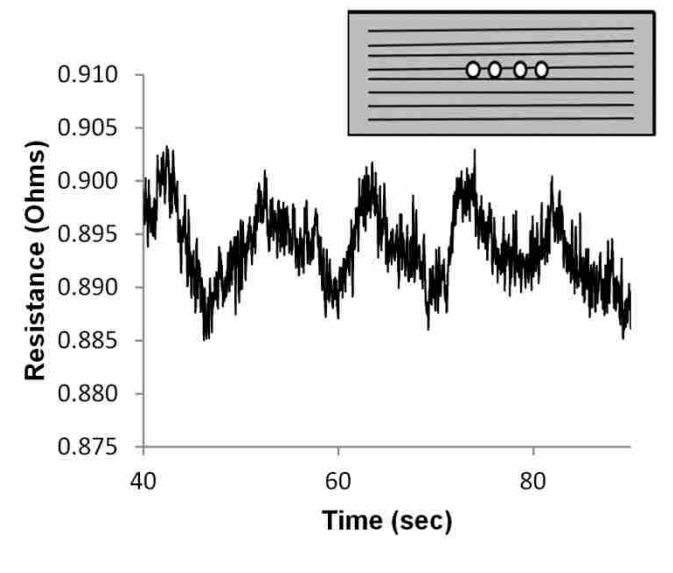

Figure 2-10: Results for collinear probing with probes oriented parallel to the outer fiber direction.

2.4.3 Box Probing

In general, the box probing method improved results as compared to the collinear probing method. An example of the feasibility of this configuration can be examined using a $[0, 90]_s$ carbon fiber layup with NCCF leading from the probes to the NiN patch. First, a control with no NCCF or NiN patch was tested. It showed no appreciable piezoresistive signal from the strain induced by the tensile tester. With the addition of the NCCF and the NiN patch a piezoresistive signal was obtained (Figure 2-11).

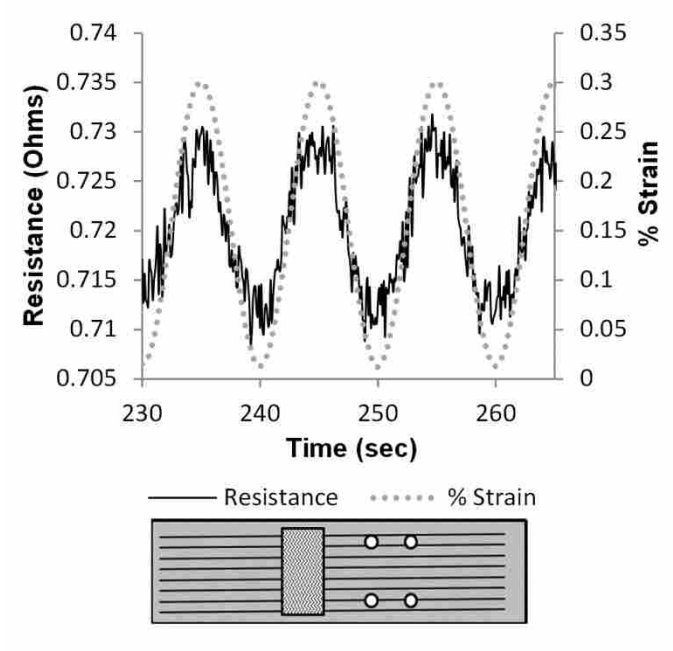

Figure 2-11: [0, 90]$_s$ layup with a NiN patch and NCCF leading from the probes to the patch. Probes were placed within 1.0 cm of the patch.

In Figure 2-11 the probes are placed in close proximity to the patch. This limits the signal from scattering across the surface of the carbon fiber. The advantage of the NCCF leads from the probe to the patch is that the more conductive NCCF does not contribute to the piezoresistive signal while encouraging the current to flow from the probes to the patch and back to the probes. This limits the amount of current flowing directly from input probe to output probe by crossing the carbon fiber. This allows one the freedom to remotely probe away from the NiN patch but still measure the strain at the patch location. An example is shown in Figure 2-12 where the patch is located 7.75 cm away from the probing location.

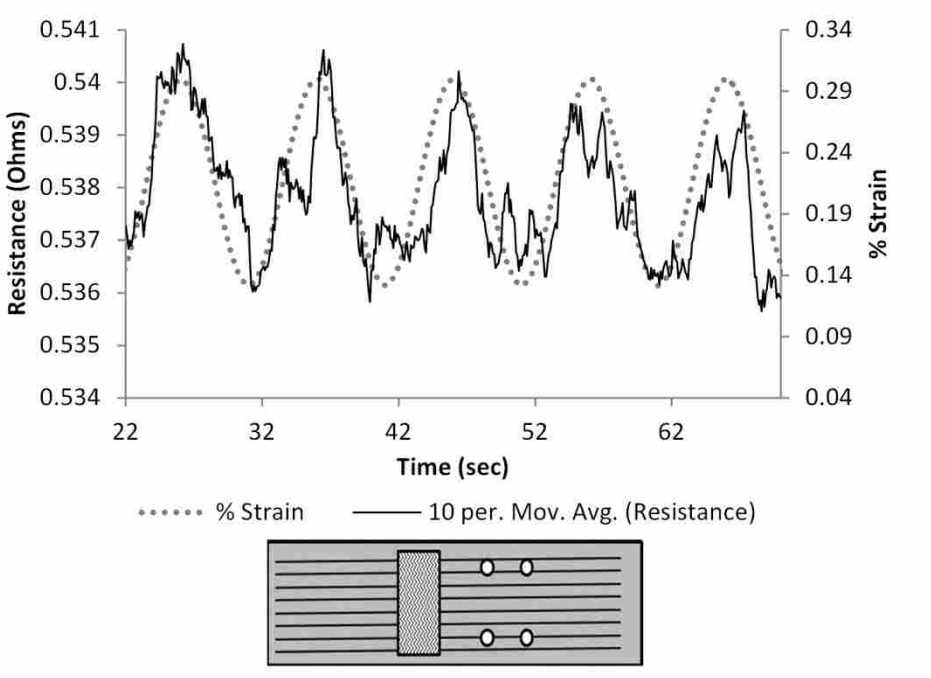

Figure 2-12: Remote box probing by using NCCF as leads from the probes to the patch.

Notice that the signal in Figure 2-12 has a moving average applied to improve the signal visibility while the signal in Figure 2-11 does not. This suggests that while remote probing is a feasible option the signal improves as the probes are placed closer to the patch. When tests were performed without NCCF leading from the probes to the patch there was no piezoresistive signal during remote probing. This result can also be seen by comparing the signal-to-noise ratio in Table 2-1.

2.4.4 Longitudinal Probing

To test the feasibility of remote strain sensing using longitudinal probing (see Figure 2-5c) two samples were originally compared. Each sample was composed of a $[90, 0]_s$ layup. The first sample was pure carbon fiber and contained no NiN patch or NCCF. No signal was obtained when straining. This suggests that remote strain sensing at large distance is impractical

with neat carbon fiber layups, or would require a much high input voltage. The second layup contained both NCCF in the longitudinal configuration and a NiN patch between the two NCCF bundles. In the second sample tests were conducted with the probes at a distance of 4 cm and 14 cm away from the patch location which can be seen in Figure 2-13 and Figure 2-14, respectively. From the results there appears to be little difference in the amplitude or clarity of the resistance signal as the distance between the probes and the patch location vary. In Table 2-1 it can be seen that both the 4 cm and 14 cm signal-to-noise ratios are relatively close with the 14 cm test actually being higher. This is attributed to the variation of clamping the probes to the specimen induced by user inaccuracy. Future research is needed to improve clamping methods to alleviate this variability.

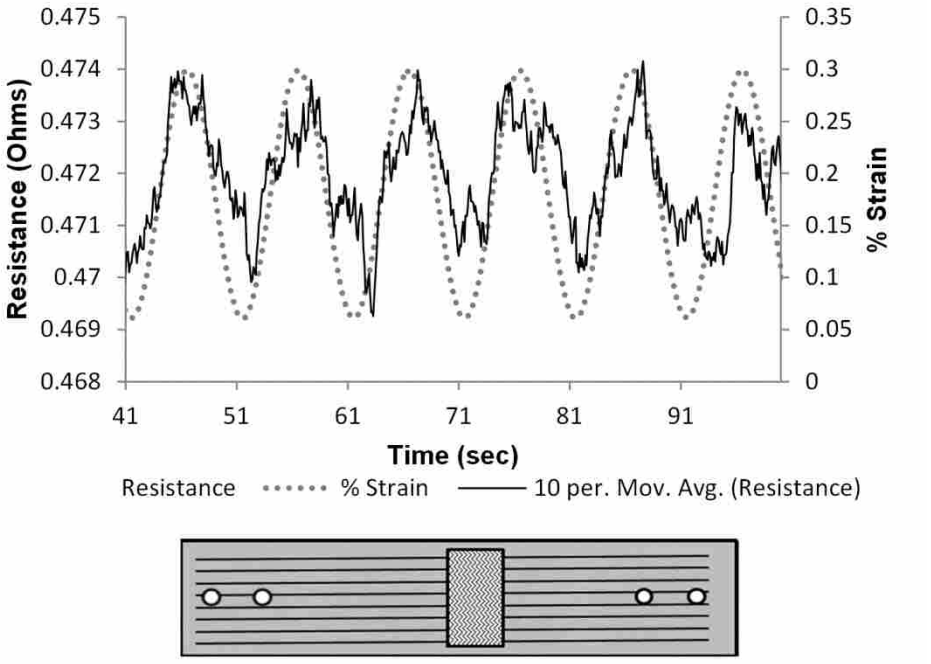

Figure 2-13: $[90, 0]_s$ layup with NCCF and NiN patch longitudinally probed with d = 4 cm.

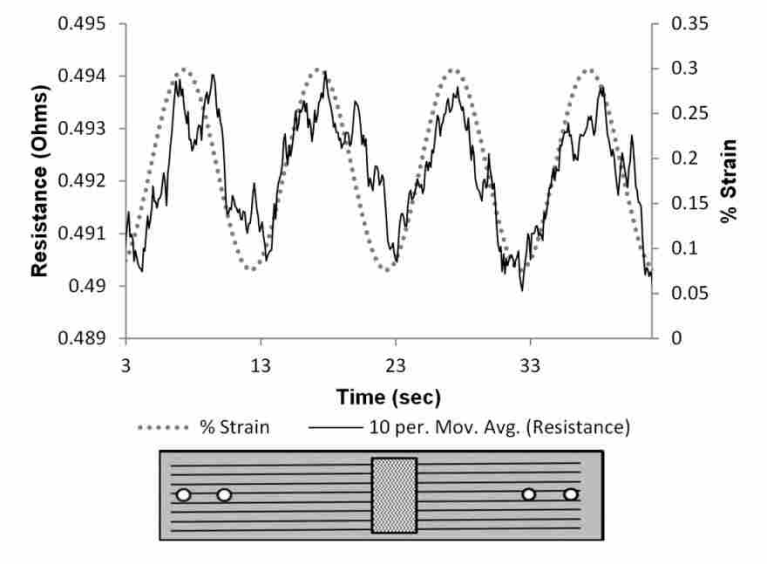

Figure 2-14: [90, 0]s layup with NCCF and NiN patch longitudinally probed with *d* = 14 cm.

The signal-to-noise ratio was calculated for each sample and can be seen in Table 2-1. Recall that a larger SNR correlates to a higher quality signal and that a value lower than about 0.30 suggests that there is no distinguishable signal that can be correlated to strain. The standard deviation was typically calculated over 3 - 4 different samples, and 2 - 4 repeat tests on a given sample.

Table 2-1: SNR calculations for various samples.

Orientation	NiN patch	NCCF	Probe Method	Distance (cm)	SNR	Standard Deviation
[0, 90, 0, 90]	No	No	Perpendicular collinear	NA	0.0518	0.043
			Parallel collinear	NA	0.8767	0.099
	Yes	No	Box	2.5	3.0018	1.202
				4	0.1454	0.022
		Yes		2.5	6.2408	2.448
				7.5	0.4556	0.049
[90, 0, 0, 90]	Yes	Yes	Longitudinal	4	0.5099	0.196
				14	0.4818	0.068
		No		14	0.2534	0.032
[0,0]	No	Yes	Longitudinal	14	0.0209	0.010

It can be seen from Table 1 that the proximity of the probes to the patch is an important factor to the piezoresistive signal strength for both box and longitudinal probing methods. Using the carbon fiber as circuitry to the strain sensor location yields a piezoresistive signal that can be correlated to strain. With the addition of the NCCF in the layup the probes can be located at greater distances away from the patch and still return a distinguishable signal, thus allowing for remote probing. Comparing the SNR values of the box probe method at 2.5 cm with and without NCCF shows that the NCCF prevents signal loss due to noise. This suggests that the nickel coated carbon fiber helps control the path of the electrical signal. These results can also be seen in the results for the box probing method at 4 cm and 7.5 cm or comparing the longitudinal method at 14 cm with and without NCCF.

The longitudinal probing allowed for remote sensing at greater distances than either the collinear or box probing methods and thus is considered as a superior probing method. It was also observed from the last test in Table 2-1 that when the fibers were oriented in the [0] direction there was no piezoresistive signal obtained (SNR = 0.0209). To verify these results and further investigate the feasibility of remote strain sensing in multidirectional carbon fiber laminates the longitudinal method was further studied.

Additional samples were prepared to be tested using the longitudinal probing method and can be seen in Table 2-2. These samples were developed to determine whether the piezoresistive signal was obtained through the carbon fiber prepreg or the NiNs embedded in the carbon fiber. Also, the orientation of the carbon fiber to the NCCF bundles was analyzed. To calculate the standard deviation two of each sample was made and tested 3 – 4 times.

Table 2-2: Tensile sample configurations and their accompanying signal-to-noise ratio (SNR) results.

Sample	Material	Patch	SNR	Stardard Deviation
A	$[0, 90]_s$ Carbon Fiber	Carbon Fiber [0]	0.93	0.28
B	$[0, 90]_s$ Carbon Fiber	NiN	1.46	0.21
C	$[90, 0]_s$ Carbon Fiber	Carbon Fiber [90]	12.54	1.44
D	$[90, 0]_s$ Carbon Fiber	NiN	3.34	0.05
E	Woven Fiberglass	Carbon fiber [90]	11.67	0.90
F	Woven Fiberglass	[90] and NiN	33.16	1.93

Figure 2-15 shows the results obtained from tensile tests performed on samples A and C. Each of these samples consisted of a carbon fiber patch with different carbon fiber orientations. In Figure 2-15a the carbon fiber on the surface and NCCF are oriented in the [0] direction. In Figure 2-15b the carbon fibers on the surface are oriented in the [90] direction while the NCCF are oriented in the [0] direction. By examining Figure 2-15a it can be seen that when the carbon fiber is oriented parallel to the NCCF the piezoresistive signal does not have a strong correlation to the strain even though the SNR is above the prescribed 0.3 threshold. This shows that the SNR metric does not define that a signal correlates to strain. The SNR value only indicates that once the signal has been observed to correlate to strain the SNR value can relate to the clarity of the signal. When carbon fibers and NCCF are oriented transverse to one another the piezoresistivity relates well to strain and a significantly higher SNR value is obtained.

The results in Figure 2-15 show that the piezoresistivity of carbon fiber can be exploited to determine the percent strain in a multidirectional laminate carbon fiber structure. Also, NCCF can be used as pseudo-wires to a patch location thus allowing strain measurement at a specific location while remotely probing from the patch location. It is further confirmed in Figure 2-16

that when the carbon fiber and NCCF are oriented parallel to one another no correlation between the piezoresistive signal and strain is found.

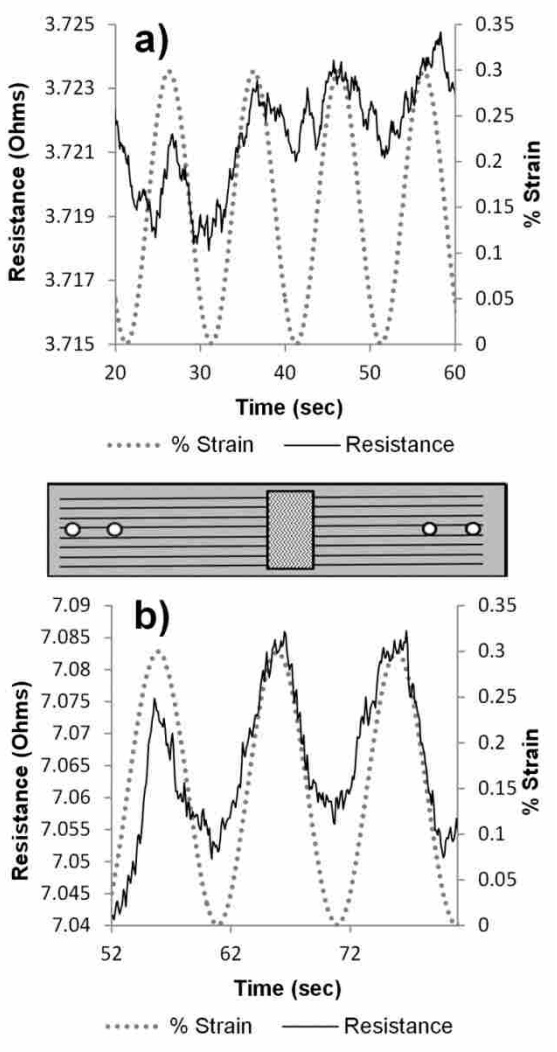

Figure 2-15: Comparison of piezoresistive signals obtained from (a) sample A and (b) sample C.

Sample B and sample D are similar to sample A and sample C except NiNs are embedded into the carbon fiber patch rather than using the carbon fiber alone as a patch. These samples were tested to determine how NiNs affects the piezoresistive signal (which has resulted in good results for other authors for long-range strain gauges)[17]. The results from Figure 2-16 yield

similar results to those in Figure 2-15. This suggests that using a NiN patch does nothing to improve upon the piezoresistive signal. Thus the relative orientation of carbon fiber in the laminate and the use of NCCF have more of an effect than using a NiN patch.

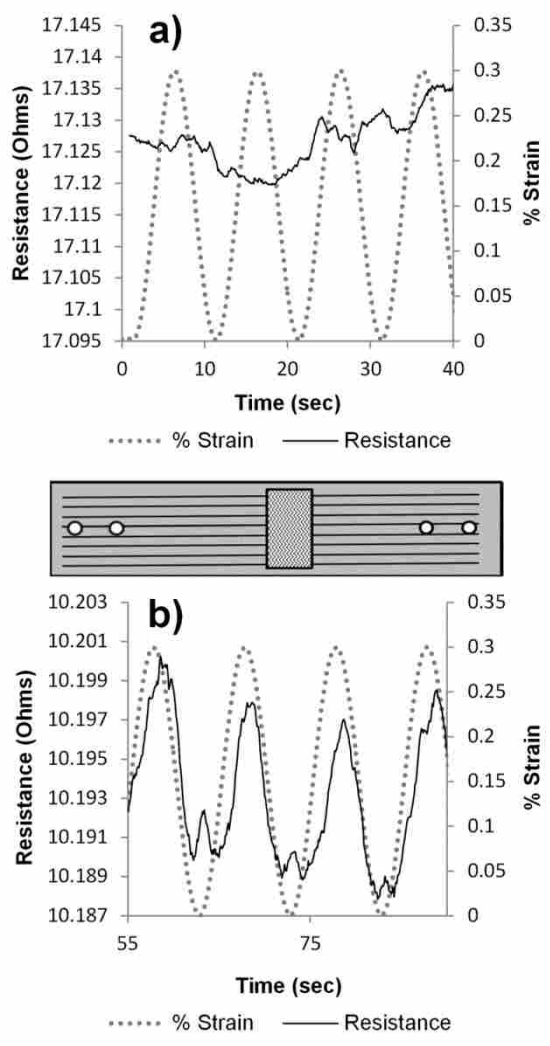

Figure 2-16: Comparison of piezoresistive signals obtained from (a) sample B and (b) sample D.

To further investigate the effect of a NiNs patch on the piezoresistive signal samples E and F were tested and the results can be seen in Figure 2-16. Each sample has a piezoresistive signal that strongly correlates to the strain which again shows that a NiN patch does little to

affect the piezoresistive signal. Table 2-2 shows a calculation for the signal-to-noise (SNR) of each sample. It is of interest to note that the signals obtained in Figure 2-17 have less noise than those in Figure 2-15 and Figure 2-16. This can be attributed to the fact that even though the NCCF is much more conductive than carbon fiber, the signal will slightly scatter across the conductive carbon fiber thus adding noise to the overall signal. In samples E and F the fiberglass is completely insulating and there is minimal scatter in the signal and the amount of noise is dramatically decreased.

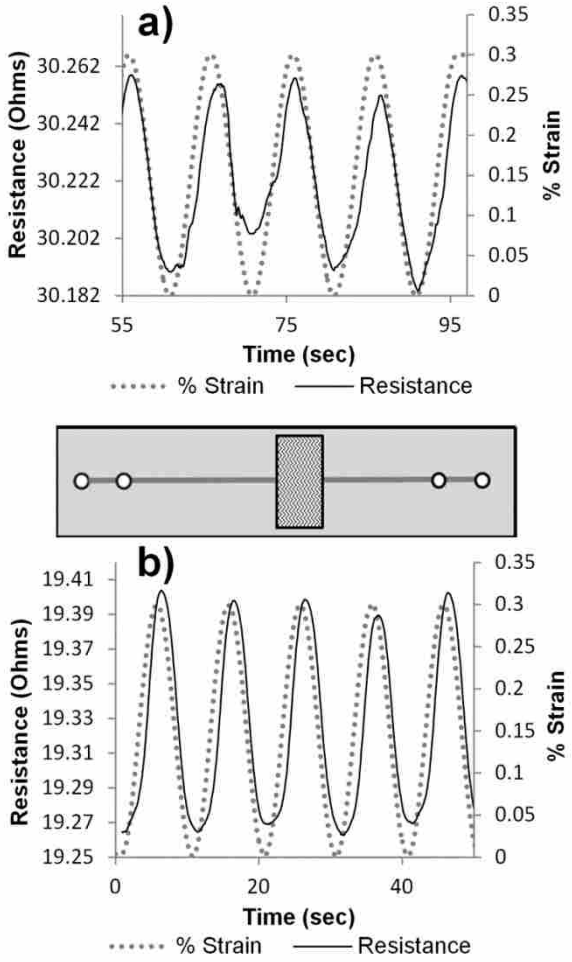

Figure 2-17: Comparison of fiberglass samples (a) E and (b) F.

2.4.5 Bending Tests

A [90, 0, 0, 90] s carbon fiber laminate with NCCF embedded on the top and bottom surfaces were placed in bending to evaluate the variation of piezoresistivity due to compressive and tensile strain (any residual strain in the sample is assumed to be negligible compared to the applied strain, as would be expected for simple laminates of this type). From Figure 2-18a increasing the displacement of the wedge caused a compressive strain on the top surface and a decrease in resistance was obtained. The opposite is true on the bottom surface; the tensile strain increased with displacement and an increase in resistance was obtained. This test demonstrates the ability to measure varying strain at different points in a sample using the NCCF circuits to pin-point the measurement site.

The three point bending test was also conducted on fiberglass Sample E from Table 2-2. Similar results were obtained and can be seen in Figure 9. The fiberglass sample once again yielded a higher signal-to-noise ratio of 24.76 as compared to the 6.79 signal-to-noise ratio of the carbon fiber, which further suggests that there is some signal loss due to the conductive nature of the carbon fiber.

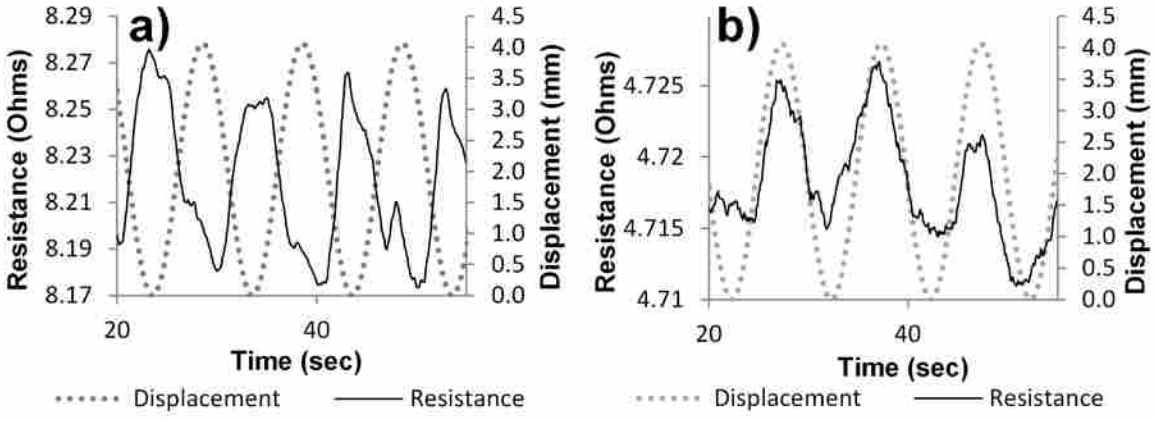

Figure 2-18: Three point bending tests on a [90, 0, 0, 90]$_s$ carbon fiber laminate with NCCF embedded on the (a) top surface (compression) and (b) bottom surface (tension).

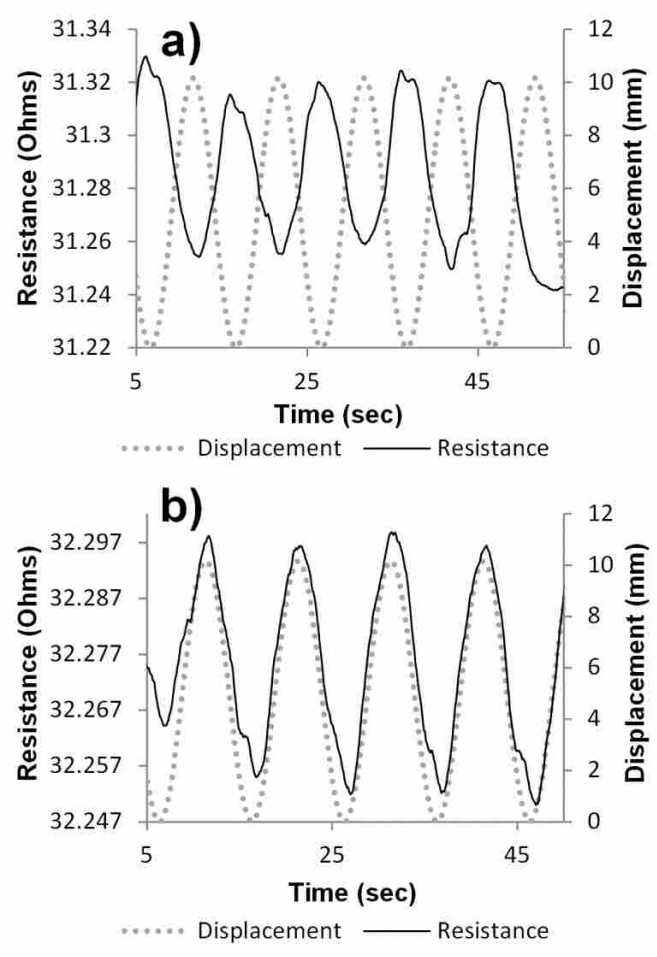

Figure 2-19: Three point bending tests results from Sample E.

2.4.6 Failure Tests

The results so far demonstrate that it is feasible to use NCCF to sense strain at a remote distance from a probing location in a sample in either tension or compression. For this to be a valid method to measure strain in a carbon fiber structure it is important to know how embedding this material affects the strength of the carbon fiber structure. Samples were embedded with NCCF and NiNs in various positions, and loaded to failure according the ASTM D3039 standard. These results were compared with samples of the same layer orientation without

embedded NiNs or NCCF. Figure 2-20 shows stress to failure for various samples with and without embedded NiNs and NCCF.

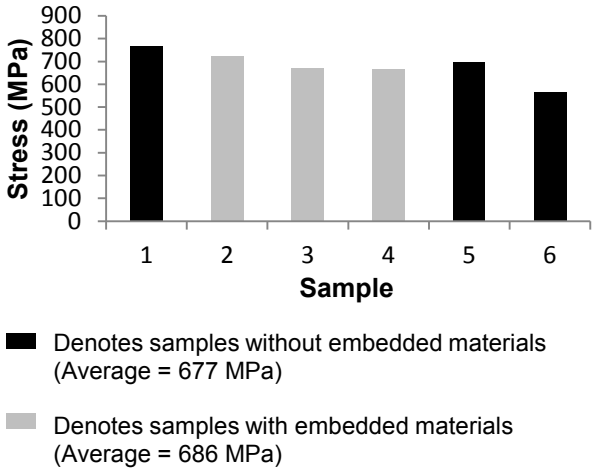

Figure 2-20: Sample 1 contains NiNs and NCCF on the top layer of carbon fiber. Samples 2 and 3 contain NiNs and NCCF embedded in the middle. Sample 4 only contains NCCF in the middle layer. Sample 5 and 6 are controls with no NiNs or NCCF.

Embedding NiNs and NCCF in the middle or top layer of a carbon fiber laminate showed no significant effect on the failure stress. Thus it is assumed that the embedded NCCF and NiNs create minimal stress concentrations in the bulk structure and these materials can be used without significantly compromising the integrity of the carbon fiber structure. A summary of these results can be seen in Table 2-3.

Table 2-3: Failure tests results

	Embedded NiNs/NCCF	No NiNs/NCCF	Total
Stress to Failure (MPa)	9578	9445	9511
Standard Dev. (MPa)	364	1179	875
% Strain to Failure	1.75	2.01	1.88
Standard Deviation	0.42	0.59	0.53

2.4.7 Pressure Vessel Application

As a proof of concept a pressure vessel was fabricated to show the feasibility and advantages of using nickel coated carbon fiber as pseudo-wires to allow remote sensing of piezoresistive carbon fiber patches. Three layers of roll-wrapped carbon fiber prepreg were laid around a 15 cm mandrel. The two interior layers were wrapped with the fibers aligned in the longitudinal direction while the outer layer was aligned in the hoop direction. Bundles of nickel coated carbon fiber were placed in the longitudinal direction on the outer surface and in the hoop direction on the interior of the pressure (see Figure 2-21). A second set of longitudinal NCCF bundles were embedded for redundancy in results. This arrangement ensured that at each sensor patch location the carbon fibers and NCCF were oriented transverse one relative to another to enable the best possible piezoresistive signal to be obtained as found in Figure 2-15 and Figure 2-16. Once cured, caps were adhered to both ends to seal the pressure vessel. Figure 2-22 shows the actual pressure vessel.

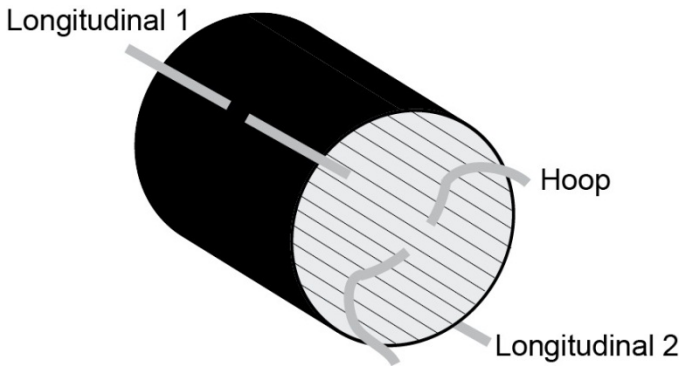

Figure 2-21: Pressure vessel design (thick grey lines represent NCCF bundles). The gap between each NCCF bundle is transverse to the carbon fiber thus allowing for piezoresitive readings.

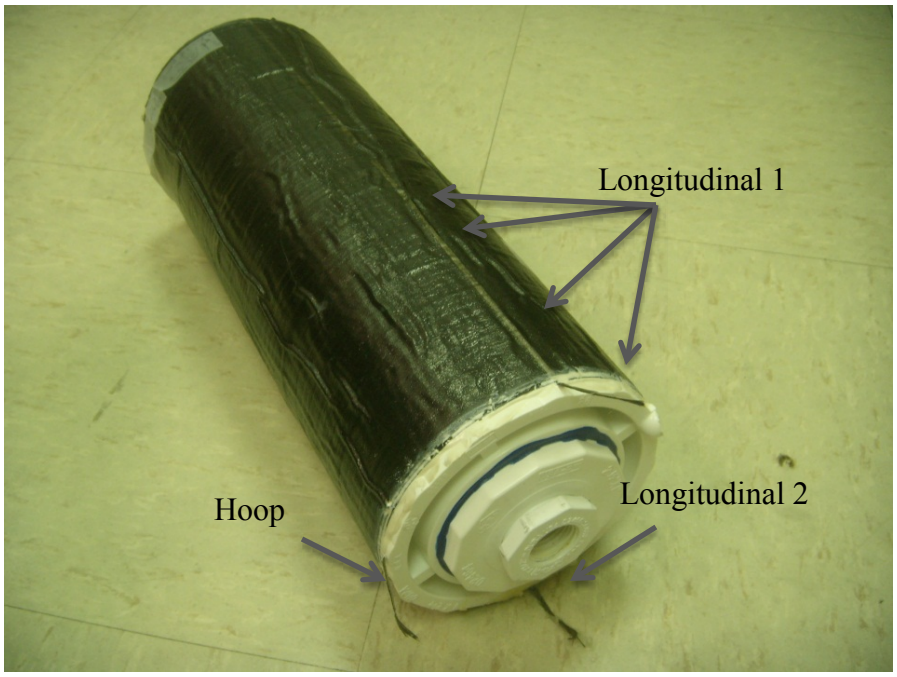

Figure 2-22: Pressure Vessel

The pressure vessel was pressurized using distilled water to prevent electrical short circuiting and alleviate safety concerns with pressurized air. The vessel was pressurized using an Ametek M&G T-65 twin seal pressure pump while resistance measurements were simultaneously being recorded. Results for longitudinal strain on the outside surface can be seen in Figure 2-23. As the pressure increased the longitudinal strain increased and an increase in the resistance was obtained. The pressure vessel was rapidly depressurized and accordingly the resistance dropped. Thus, as expected, with a tensile strain in the longitudinal direction the piezoresistive signal is positive.

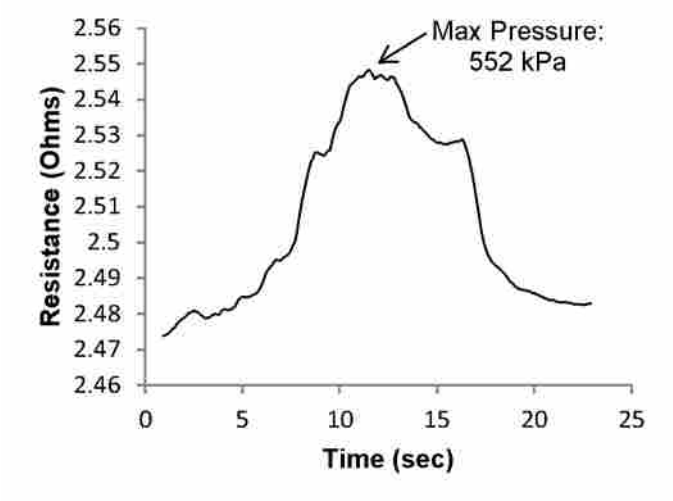

Figure 2-23: Longitudinal strain measurement in pressure vessel. The vessel was pressurized to 552 kPa and then rapidly depressurized starting at approximately 12 sec.

The results measuring the hoop strain on the interior surface can be seen in Figure 2-24. It was assumed as the pressure increased there would be a tensile strain in the hoop direction and thus a positive piezoresistive signal would be obtained, yet the results show a negative piezoresistive signal with increasing stress. These results are being attributed to the compression of the longitudinal carbon fibers in the radial direction. As the pressure increased the carbon fibers were compressed into intimate contact with one another creating a lower resistance (see Figure 2-25). Unfortunately, the data recording was interrupted before complete depressurization and subsequently the vessel was damaged so a return of the resistance reading to its unpressurized state was not seen. Yet, the results still indicate a negative piezoresistive signal in the hoop direction.

From the resistance measurements obtained it is evident that using NCCF as pseudo-wires to a patch location can allow for remote strain measurements in a carbon fiber structure. Measuring longitudinal strain creates a positive piezoresistive signal while measuring hoop strain yields negative piezoresistivity.

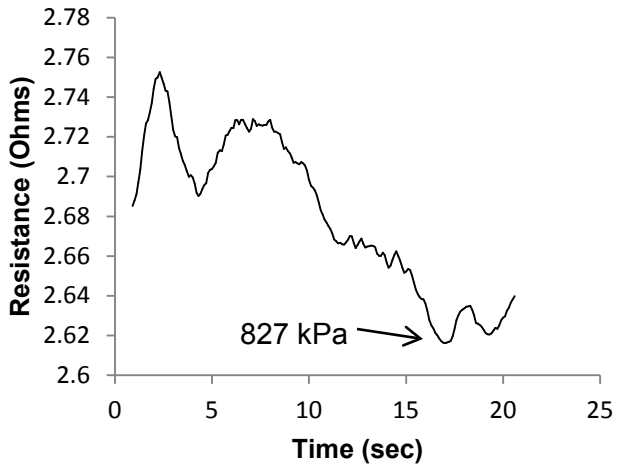

Figure 2-24: Strain reading on inside surface of pressure vessel. Pressure reached a max of 827 kPa at approximately 17 seconds. The data beyond 21 seconds was not logged due to operator error.

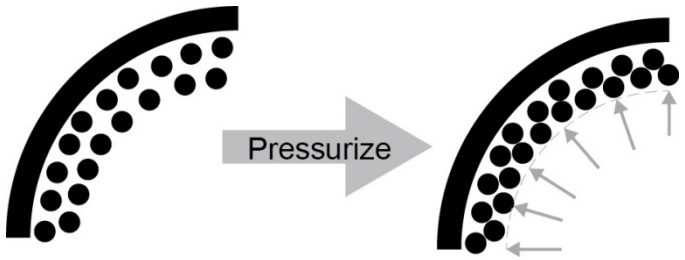

Figure 2-25: Pressure causes the fibers to compress thus lowering the resistance in the hoop direction.

Further loading the pressure vessel above 827 kPa caused the vessel to start failing. Resistance measurements were taken on both longitudinal bundles and the hoop bundle as the pressure vessel began to fail. In Figure 2-26 it can be seen as the fibers began to delaminate and break large resistance changes were detected. It is evident that this method of strain measurement could be used to detect failures within a carbon fiber component. The different amplitudes of resistance changes between the three locations could suggest the location of where failure began.

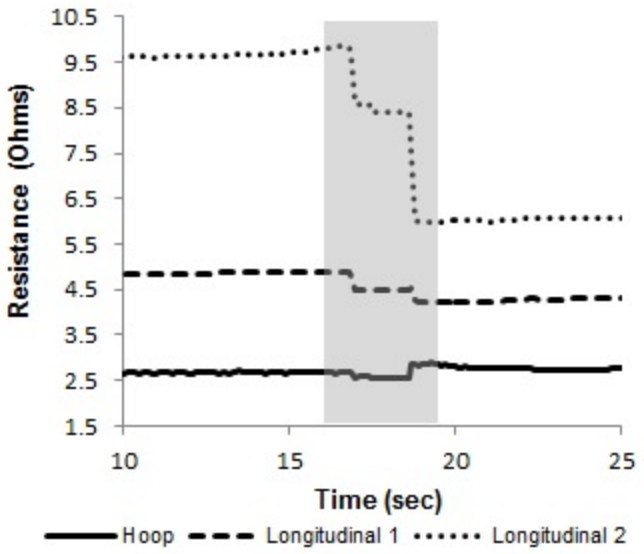

Figure 2-26: Extreme piezoresistive changes when failure occurs (gray region) suggest that failure can be detected in a carbon fiber structure.

2.5 Conclusions

A brief overview of the results from this chapter is summarized in the following bullet points, and then explained in more detail:

- Both sensor circuitry and sensor material have been evaluated
- Nickel coated carbon fiber is not piezoresistive
- Nickel nanostrands do not improve upon piezoresistive signal in multidirectional laminates
- Longitudinal probing was the most successful method for remote sensing
- Nickel coated carbon fibers act as pseudo-wires and allow for larger distances between the sensor and the probes
- Embedding nickel coated carbon fiber and nickel nanostrands into a carbon fiber prepreg do not severely weaken the structure
- Failure can be detected using the developed strain sensing technique

Embedded nickel nanostrands and nickel coated carbon fiber were evaluated as tools for in-situ strain sensing in a multidirectional carbon fiber laminate. Tests were conducted via altering of the strain sensor patch and the connecting circuitry. Previous research has used the piezoresistivity of directly embedded nickel nanostrand nanocomposites to measure strain in unidirectional layup. Testing a variety of strain sensor configurations has shown that directly embedding nickel nanostrands into a multidirectional laminate is ineffective for strain measurement and does little to improve upon the piezoresistivity of the carbon fiber.

Carbon fiber's piezoresistivity is a good measure of strain, and thus a valid strain sensor, but if the carbon fiber is also used as the current carrier to a probe location, the probing location must be extremely close to the area where strain is to be measured to allow a discernible electrical signal to be obtained. The more conductive nickel coated carbon fiber does not have the same piezoresistive properties as carbon fiber and hence is a better choice for supplying a circuit from the sensor area to the probe location. Using NCCF as the connecting circuitry provides pseudo-wires to remotely measure the strain at a desired location without piezoresistivity in the circuit affecting the signal.

It has been shown that the best results are obtained when the NCCF circuit is oriented perpendicular to the carbon fibers that are in the sensor region. Furthermore the optimal probe geometry involves the four-probe longitudinal method. Future work will be performed to determine if embedding the NCCF circuit between layers can accurately determine strain from arbitrary positions within a sample.

Samples embedded with nickel coated carbon fiber and nickel nanostrands were loaded to failure in tension to determine the adverse effects these materials have on the strength of the carbon fiber. It has been shown that the embedded materials do not significantly alter the

strength of the structure. Thus, using embedded NCCF is a safe, easy way to remotely measure strain within a carbon fiber structure without compromising structural integrity.

In addition to tensile and bending tests of laminates, a pressure vessel was built as a proof of concept application of remote strain sensing using embedded nickel coated carbon fiber for the connecting circuit. W hen pressurized, longitudinal and hoop strain were detected. Longitudinal strain yielded positive piezoresistive results while hoop s train yielded negative piezoresistive results. It was also found that when the pressure vessel began to fail the failure was detected through an extreme change in the resistance reading.

In conclusion, embedded nickel nanostrands are ineffective and unnecessary to measure strain in a multidirectional laminates. Nickel coated carbon fiber allows for remote strain sensing of a desired patch location within carbon fiber structure as long as the NCCF is oriented transversely to the carbon fiber. In addition, the NCCF does not adversely affect the strength of the carbon fiber structure in which it is embedded.

3 INTERROGATING THE PROPERTIES OF NANOJUNCTIONS IN CONDUCTIVE NANO-COMPOSITES

3.1 Percolation Theory

Percolation theory is commonly based upon a distribution of points called "sites." Between two sites there is a certain probability that a connection between those sites exists. Those connections are called "bonds." As the number of bonds increases a percolation threshold will be reached resulting in a continuous connection from one end of the volume to the other [31]. The electrical conductivity through the volume is related to how far the material is (in terms of fraction of sites that are connected by bonds) from the percolation threshold; the conductivity increases rapidly as the percolation threshold is passed. In reference to a conductive nanocomposite, the filler particles are the "sites" in percolation theory and the nanojunctions (contact points) between particles are the "bonds" (see Figure 3-1).

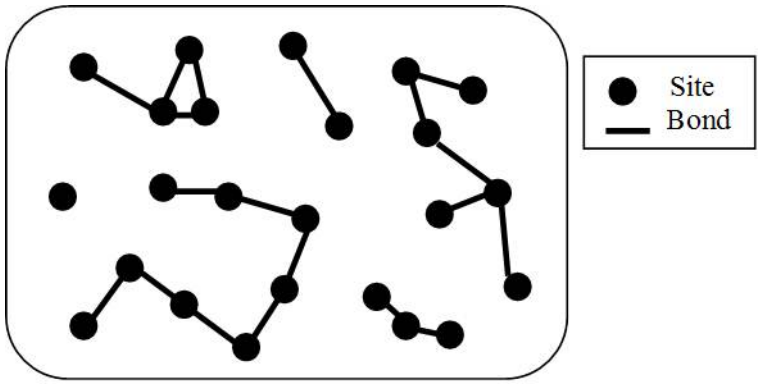

Figure 3-1: Example of sites and bonds in a percolation model (courtesy of Johnson)

The percolation threshold can be correlated to the volume fraction of conductive nanoparticles due to the increases probability of bonds forming between sites. This relation is shown in the classical percolation equation given by Equation 3-1:

$$\sigma_c = \sigma_f (f - f_c)^t \tag{3-1}$$

where σ_c is the effective conductivity of the composite, σ_f is the conductivity of the filler, t is a conductivity exponent, f is the filler volume fraction and f_c is the critical volume fraction for percolation to occur [32].

3.2 Quantum Tunneling

The percolation model requires that quantum tunneling occur to create the bonds which are essential for a conductive network in the nanocomposite. Quantum tunneling determines the existence of a conductive bond between two filler particles. When an electron flows through one of the conductive nano-particles and reaches a barrier, such as a bulk insulating polymer, there is a certain probability that the electron will actually tunnel through the barrier, thus creating a nanojunction [18]. The probability of quantum tunneling occurring greatly increases with a decrease in distance between two adjacent sites. This distance generally must be less than about 5 nm [21].

As the number of conductive nano-fillers (or sites) increases in a constant volume, the closer they will be packed, thus increasing the probability of creating a highly conductive bond between sites. Furthermore, as the material is strained in tension, the gaps between adjacent nanostrands vary slightly, increasing or decreasing (via Poisson contraction) the local conductivity; i.e. possibly opening or closing a bond between the strands. Such variation close to

the percolation threshold correlates to a dramatic change in the overall resistance of the nanocomposite.

The tunneling resistivity in the barrier between two conductive particles is:

$$\rho_G = \frac{h}{e^2}\frac{1}{k_0}\exp(2\pi k_0 \delta) \quad \text{with}$$

$$k_0 = \frac{2\sqrt{2m_e\lambda}}{h} \tag{3-2}$$

where h is the Planck constant (J s), e is the charge of an electron (C), m_e is the mass of an electron (kg), k_0 describes the potential barrier, λ is the barrier height (J), and δ is the junction distance (m) [33].

Thus quantum tunneling and percolation is dependent on the barrier height λ and the junction distance between conductive nanostrands δ. Additionally, percolation is dependent upon a connecting network of bonds across the nanocomposite which can be correlated to the volume fraction of conductive filler particles (Equation 3-1). Assuming that the number of highly conductive bonds in a percolating nanocomposite is constant above the percolation limit, the conductivity and piezoresistivity of the nanocomposite will depend only on the barrier height and junction distance. The molecular interaction of the insulating polymer between nanostrands dictates the barrier height as well as the junction distance between strands. With the knowledge of the junction distance and the barrier height for individual polymers an accurate percolation model for nickel nanostrand filled nanocomposites can be obtained.

The junction distance between particles depends heavily upon the interaction of polymer chains with the nanoparticle. The portions of the polymer chains closest to the particle become immobilized or bound to the surface of the particle [34]. This layer is called the adsorbed layer

and its thickness can been calculated using nuclear magnetic resonance [35], TEM coupled with scanning tunneling microscopy [36], TEM coupled with thermal gravimetric analysis methods [37], and dissolution methods [38]. Each of these methods assumes that the junction distance is twice the adsorbed layer thickness. Kluppel et al. discovered that by simply measuring the permittivity vs. frequency curves with dielectric spectroscopy the average junction distance between nanoparticles can be obtained [39, 40]. When the volume fraction of filler causes the amount of conductive bonds to be above the percolation limit it is assumed that this method will yield junction distances that are near the minimum junction distance. Dielectric spectroscopy has been used to measure the junction distance with carbon black [41] and carbon nanotube [33] nanocomposites and has shown to vary with polymer. No such study currently exists for nickel nanostrand nanocomposites.

Studies have shown that holding all variables constant but altering the barrier material in the gap between conductive particles alters the tunneling resistance [42]. This suggests that the barrier height is dependent on the barrier material. Thus to accurately model the conductivity of a nanocomposite it is essential to know the barrier height of the polymer used in the composite. Numerous studies have used scanning tunneling microscopy (STM) to measure the barrier height of a substance [43, 44]. With this technique, barrier height determination requires an aqueous solution to represent the barrier material. This can be a limitation for many complex materials, both in terms of sample preparation and application of the aqueous measurement to the actual solid composite. Johnson et al. implemented a new method described as nanoindentation tunneling microscopy (NTM) to calculate barrier heights in solid barrier materials (e.g. cured polymer) [13]. In this indentation method, a conductive tip is pressed through a thin film of the

material and into a conductive substrate while the instrument measures the gap distance and conductance simultaneously.

Here, we present an extension of O. Johnson et al. to calculate barrier heights for common and complex polymer materials of interest for formulation of nickel nanocomposites. Barrier height measurements of the pure polymers are complemented with dielectric measurements of NiN-filled polymers to calculate junction distance. By combining these two techniques we can qualitatively determine the potential of the various polymers for large-scale NiN composite manufacture.

3.3 Experimentation

3.3.1 Sample Preparation

The polymers studied are widely available commercial products described in Table 3-1. These polymers have the advantage of being easy to use, relevant to commercial applications, and previously studied in NiNs nanocomposite systems [26]. The dielectric measurements required polymers which contained dispersed NiNs, forming a percolating conductive nanocomposite. To each polymer was added 15% volume fraction of NiNs to ensure each nanocomposite was above the percolation limit which ranges from 3 – 6 % depending on the polymer. The dispersion was accomplished by adding NiNs and solvent (if necessary) to the uncured polymer. The solvents used for each polymer are given in Table 3-1. The uncured nanocomposites were placed into molds to create dielectric disc shaped samples that were 1 inch in diameter and between 0.05 and 0.1 inches thick. The polymers were then cured according to the manufacturer's specifications.

Table 3-1: Polymers used in this study with accompanying solvents used for processing

Name	Manufacturer	Type	Processing Solvent
Polycrylic®	Minwax®	Acrylic/Urethane	Water
Desothane® HS CA8201/F Clear	PRC-DeSoto	Urethane	Methyl Ethyl Ketone (MEK)
Armorseal® 1000 HS clear	Sherwin Williams®	Epoxy	MEK/Xylene/Ethanol
Sylgard 184	Dow Corning®	Silicone	Xylol
CARC Clear MIL-DTL-64159 Ty II	Spectrum Coatings	Aliphatic Polyurethane	Water
Irogran® PS455-302P (IRO)	Huntsman	Thermoplastic Polyurethane (TPU)	Tetrahydrafuran (THF)

Barrier height measurements of the pure polymers required extremely small amounts of polymer in order to simulate the nanometer scale gap distances commonly found in most conductive nanocomposites. This was accomplished by depositing thin films of the polymers onto nickel substrates. Nickel substrates were polished with standard slurry polishing procedures followed by a final electropolishing step in order to minimize surface roughness. Substrates were then cleaned with an acetone wash and five minutes of atmospheric plasma etching immediately prior to coating. Polymer films were fabricated on the nickel substrates by use of a controlled dip-coating procedure which has been previously established to create nanometer-scale organic films [45]. Briefly, the polymers of interest were dissolved in appropriate organic solvents (Table 3-1) to create solutions of approximately 1 wt%, and the nickel substrates were dipped into and removed from the solutions in humidity-regulated room temperature environment at a constant speed of 25 mm/min. The samples appeared dry after several seconds but were allowed to dry for a minimum of 24 hours before analyzing. The thicknesses of the polymers were measured by a variable angle spectroscopic ellipsometer (VASE) from J.A. Woolam Co., Inc

(Lincoln, NE). For a general review of thin film ellipsometry, please refer to Theeten and Aspnes [46].

3.3.2 Barrier Height Measurement

For the purposes of nano-composites or other conductor-insulator-conductor systems, the barrier height λ is defined as the energy difference between the conduction band of the insulator and that of the conductor. Equation 3-2 shows the interrelationship of λ with the potential barrier k_0, the junction distance, and the tunneling properties of the composite. To obtain λ for the polymers, a conductive nanoindentation scheme was used which was based on but modified from previous work [47]. The modified indentation method is an improvement in data quality and noise reduction. H ere, a Hysitron TriboIndenter is used in conjunction with a boron-doped conductive diamond tip and conductivity measurement software (nanoECR®), measuring the current or voltage between the tip and the substrate continuously during indentation. A standard gold specimen was used for calibrating the system at an applied bias of 1 V, and a typical current vs. depth (S) curve is shown in Figure 3-2.

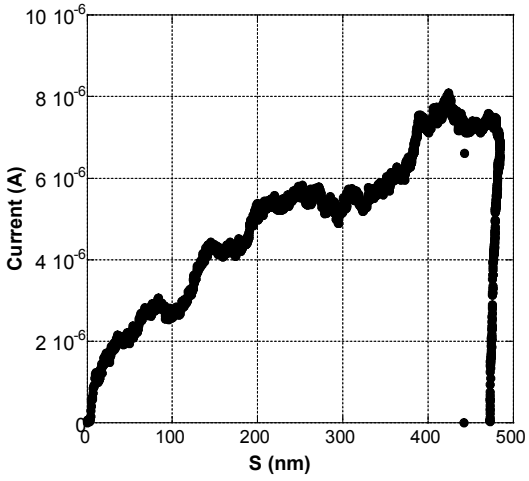

Figure 3-2: Current as a function of indentation depth for gold at 1V.

Traditional explorations of barrier height phenomenon describe tunneling theory in terms of conductance, though here current is used. The tunneling conductance equation is

$$G = G_0 \exp(-1.025\sqrt{\lambda}s) \tag{3-3}$$

where G_0 is the conductance when the plate and tip are in contact, λ is the barrier height, and s is the distance from indenter tip to plate [42]. Linearizing Equation 3-3 the following is obtained:

$$\ln(G) = -1.025\sqrt{\lambda}s + \ln(G_0) \tag{3-4}$$

Thus with knowledge of the conductance as a function of gap distance the barrier height can be calculated from the slope of an ln(G) vs s plot. Where the slope (m) is

$$m = -1.025\sqrt{\lambda} \tag{3-5}$$

Using the linear regression to solve for the slope the mean barrier height can be obtained:

$$\lambda = \left(\frac{m}{-1.025}\right)^2 \tag{3-6}$$

The nanoECR setup measures current as a function of depth for a given voltage, or voltage as a function of depth for a given current. The software provides an excellent way to obtain conductance data: indentation is performed to a given depth, at which point an I-V sweep is performed. However, it is assumed the results given by this method were unreliable for the very thin and compliant polymer films due to the difficulty of finding the exact surface and the possibility of creep of the polymer while the indenter was held at a given depth. Both factors would significantly convolute the data. Thus, it was decided to keep the accurately measured current vs. depth data and assume the voltage varied linearly (from 0 to the applied bias) over the junction distance. This assumption was considered valid based on previous experience, in which

the voltage was approximately exponential over the course of the entire indent but largely linear over the range of interest [47].

A typical current vs. depth plot is shown is Figure 3. For all the thin polymer samples, the initial jump in current represents the moment that electrons from the conductive tip tunnel through the polymer. Subsequent variations in the current occur well after the indenter has completely passed through the polymer and into the nickel. Inset into Figure 3 is a magnified view of the initial current jump, along with a linear fit for the data. The voltage is assumed to vary linearly over the approximately linear current region.

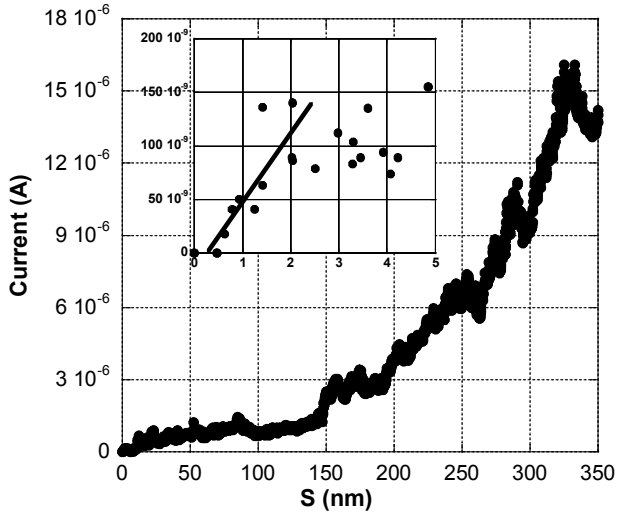

Figure 3-3: Current vs. depth for a typical indent into CARC-coated Ni sample. The initial increase in current (inset) represents the tunneling current before the tip has penetrated the polymer and contacts the Ni.

Table 3-2 gives the polymers that were tested in this way, along with the thickness values from ellipsometry and the calculated barrier heights.

Table 3-2: Polymers tested with conductive indentation.

Name	Thickness (nm)	Barrier Height (eV)
Polycrylic®	26.1 ± 4.1	0.9 ± 0.5
Desothane® HS	10.5 ± 0.9	1.7 ± 0.9
CARC	22.7 ± 3.7	0.9 ± 0.7

It is noted that barrier height ranges for several polymers fall in the 0.3 – 1.5 eV range [48]. While the Desothane sample has a slightly elevated barrier height, it is felt that the values for all the polymers are sufficient for first order calculations. In the future subsequent experiments will be attempted to reduce the error (caused by variability between indents and sample size).

3.3.3 Junction Distance Measurement

The junction between conductive nanoparticles in a nanocomposite has been modeled as a resistor and capacitor circuit in parallel, as is illustrated in Figure 3-4 [33, 41, 49-51]. In this model the dielectric response is treated as a network of these resistor-capacitor circuits.

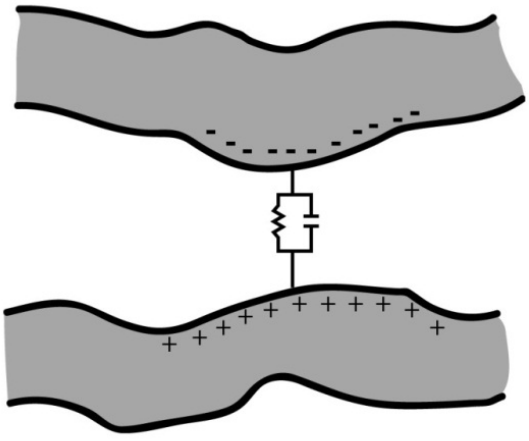

Figure 3-4: Parallel resistor and capacitor of nanojunctions.

With this circuit model the characteristic frequency at a nanojunction is

$$\omega_c = \frac{1}{RC} \tag{3-7}$$

where ω_c is relaxation frequency, R is the resistance, and C is the capacitance. For capacitance

$$C = \frac{\varepsilon_0 \varepsilon A}{\delta} \tag{3-8}$$

where ε_0 is the electric constant, and ε is the relative permittivity (often referred to as the dielectric constant). Inserting Equation 3-8 and Equation 3-2 into Equation 3-7 we get

$$\omega_c = \frac{3e^2}{16\pi^2 h\varepsilon_0}\frac{k_0}{\varepsilon}e^{-k_0\delta} \tag{3-9}$$

Thus with knowledge of the characteristic frequency, ω_c, the junction distance, δ, can be calculated.

To obtain the characteristic frequency the relative permittivity is needed at various frequencies. An HP model 4192A impedance analyzer with a frequency range of 5 Hz to 13 MHz was used. Stray admittance and residual impedance are sources of error with this equipment. To eliminate these errors an HP 16451B dielectric test fixture for dielectric constant measurement of solid materials was attached. The electrode used in this fixture was a 5 mm guarded electrode which eliminates edge capacitance error.

Depending on the polymer used there was varying amount of roughness and compressibility in the samples being tested. To prevent these variables from affecting the results, a non-contacting electrode method was used per the manufacturer's specifications. In this method two tests are ran using the analyzer, one with the sample between the parallel plates

of the analyzer and the other without the sample between the plates (see Figure 3-5). The relative permittivity can then be calculated using Equation 3-10.

$$\varepsilon_r = \frac{1}{1 - \left(1 - \frac{C_{s1}}{C_{s2}}\right)\frac{t_g}{t_a}} \tag{3-10}$$

Where ε_r is the relative permittivity, C_{s1} is the capacitance without the sample inserted, C_{s2} is the capacitance with the sample inserted, t_g is the junction between electrodes, and t_a is the thickness of the sample.

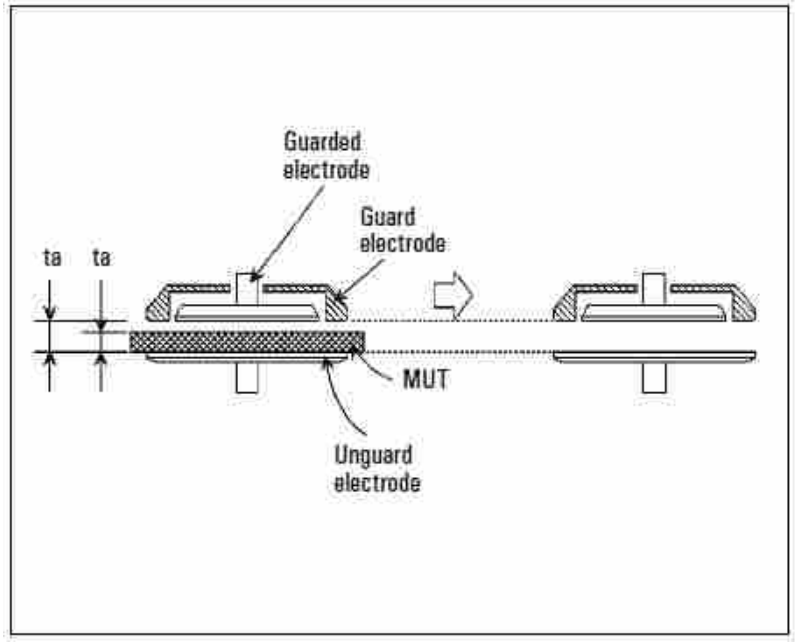

Figure 3-5: Non-contacting Electrode Method. From the manufacturer MUT stands for Material Under Test and is called the sample in this research. (Image obtained from user manual [52])

Measuring the relative permittivity with a broad range of frequencies the Cole-Cole equation (Equation 3-11) can be used to fit the dielectric data [53]. The fit yields values for the relaxation time τ, the relaxation strength $\Delta\varepsilon$, and the broadness parameter α. Since $\omega_c = 1/\tau$ the

characteristic frequency, ω_c, can be obtained and plugged into Equation 3-9 and the junction distance can be evaluated.

$$\epsilon(\omega) = \epsilon_\infty + \sum_j \frac{\Delta\epsilon_j}{1 + \left(i\omega\tau_j\right)^{\alpha_j}} \tag{3-11}$$

The permittivity results obtained from the dielectric measurements can be seen in Figure 3-6 with the accompanying fits for each polymer. The relaxation process that is observed at high frequencies is caused by the relaxation of charge carriers at the polymer/nanostrand interface due to field reversal. It is evident from Figure 3-6 that the frequency and strength of the relaxation process is heavily dependent on t he polymer showing that the adsorbed layer thickness is polymer dependent. The measured relaxation transition occurs at higher frequencies in the order of $\omega_{Syl} < \omega_{IRO} < \omega_{CARC} < \omega_{Des} < \omega_{Arm} < \omega_{CP1} < \omega_{Poly}$. It is noted that for the relaxation curves for Polycrylic, Armorseal, and CP1 that the relaxation process is not as dramatic as the other polymers at the maximum frequency range of the measuring equipment. Regardless, using the Cole-Cole equation the fitted line can be extrapolated to give the relaxation frequencies for these polymers.

The junctions distances are in the opposite order of the relaxation frequencies where $s_{Syl} > s_{IRO} > s_{CARC} > s_{Des} > s_{Arm} > s_{CP1} > s_{Poly}$, which can be seen in Table 3-3. It is assumed that the adsorbed layer is half of the measured junction distance.

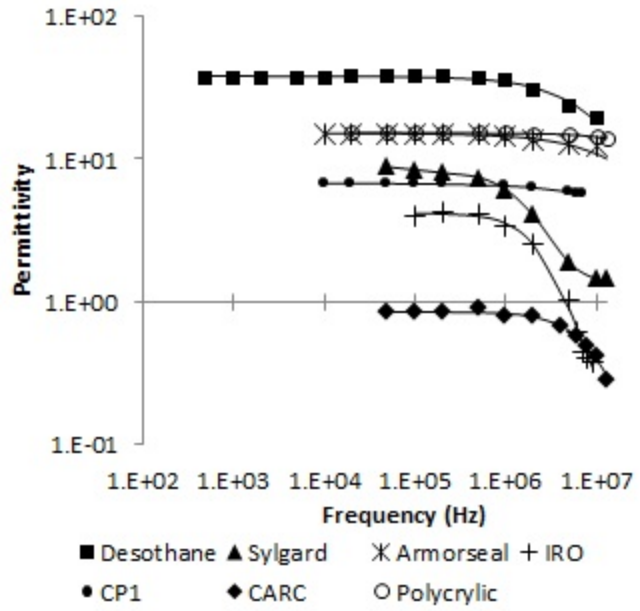

Figure 3-6: Permittivity measurements (markers) with accompanying fits (solid lines) for various polymer filled with 15% volume fraction of NiNs.

It is assumed, as in previous research, that the barrier height is 0.3 eV and the dielectric constant is 3 for each polymer [16, 33, 41, 54, 55]. One exception is the Sylgard polymer in which the barrier height is 0.28 eV [13] and the dielectric constant is documented at 2.65 [56]. With these values the junction distance can be calculated. Comparing the measured junction distances using the assumed barrier height from Table 3-3 and the resistivity measurements at 0 % volume fraction of nanostrands in Figure 3-7 it is noticed that the polymers with higher junction distance values have a higher resistivity. This suggests that neat polymers with a higher resistivity correlate to a larger adsorbed layer thickness on the nickel nanostrands.

Table 3-3: Fitted parameter values and calculated barrier height and junction distance for various polymers.

Polymer	ω_c(MHz)	α	Δε	λ (eV) Assumed/Measured	δ (nm) (assumed λ)	δ (nm) (measured λ)
Polycrylic	67.2	0.8846	15.26	0.3/0.9	2.66	1.56
CP1	43.9	0.6733	6.774	0.3/NA	2.74	--
Armorseal	25.6	0.7112	15.2	0.3/NA	2.83	--
Desothane	9.37	0.7456	38.17	0.3/1.7	3.01	1.31
CARC	9.21	0.9336	0.8513	0.3/0.9	3.01	1.77
IRO	2.48	0.9763	4.18	0.3/NA	3.20	--
Sylgard	1.83	0.7562	9.001	0.3/0.28*	3.25	3.28

* Measured by Johnson [25]

The measured barrier heights of the three polymers evaluated in this research: Polycrylic, Desothane, and CARC (see Table 3-2) are significantly higher than the assumed value and the previously measured value for Sylgard. This caused the junction distance to decrease to the ~1 nm range which is an approximate proximity needed for quantum tunneling to occur as claimed by other researchers [13, 21]; suggesting that these measured barrier height values are more accurate than the previously assumed value of 0.3 eV. Additionally, the improved nanoindentation techniques yield more feasible results.

Resistivity measurements were taken for each sample and compared to the percolation curves developed by Hansen et al in Figure 3-7 [57]. From Table 3-4 it is evident that there is no correlation between the resistivity measurements obtained in this research and those of Hansen. These incongruous results are attributed to the surface resistivity being measured on thin films in Hansen's work while this research measured the bulk resistivity through the sample thickness.

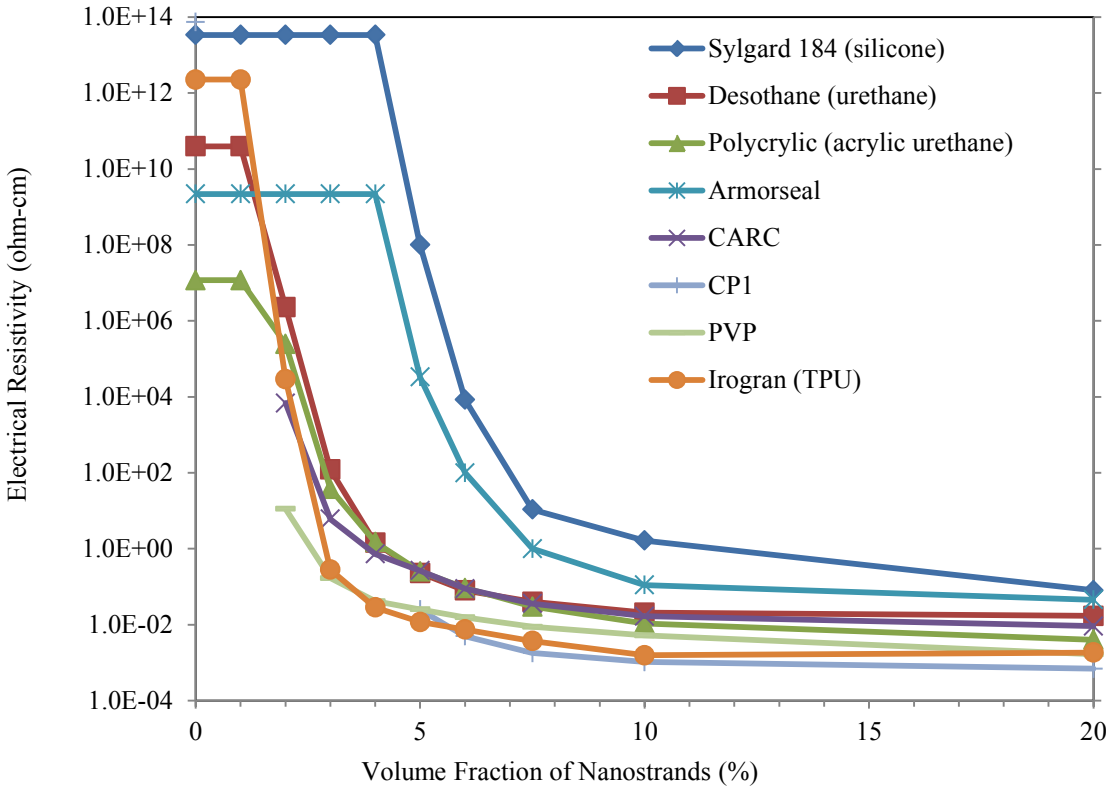

Figure 3-7: Percolation curves for nickel nanostrand nanocomposites. (Plot taken from Hansen which has been submitted to be published [57])

With measured resistivity of the 15% NiN filled polymers and knowledge of the barrier height a calculated value for the junction distance can be obtained and compared to the measured value. T he calculated junction distance values are slightly smaller yet line up well with the measured junction distances. It is noted that for unknown reasons the resistivity measurements for CP1, Armorseal, and Desothane were extremely unreliable and not used to calculate a junction distance.

Table 3-4: Resistivity measurement comparison

Polymer	Bulk Resistivity (Ω m)	Surface Resistivity by Hansen (Ω m)	Calculated Junction Distance (nm)
Polycrylic	71.989	7.4	2.50
CP1	NA	0.85	NA
Armorseal	NA	78.3	NA
Desothane	NA	18.9	NA
CARC	141.37	12.9	2.62
IRO	1031.6	1.75	2.98
Sylgard	1680.6	866.1	3.16

The main motivation behind finding the barrier height and typical junction distance in a polymer is in order to model the physical properties of a composite, and perhaps design better materials. In the case of the materials discussed in this paper, the physical property of greatest concern is the bulk resistivity of a NiN filled nanocomposite. Using Equation 3-2 yields the tunneling resistivity at a single nanojunction, but not for the bulk nanocomposite. In order to relate the junction resistance to bulk resistance of the nanocomposite, it is assumed (for simplicity) that there is a linear relationship between the bulk resistivity and the nanojunction resistivity as defined in Equation 3-12:

$$\rho_{\text{bulk}} = m\rho_{junction} \tag{3-12}$$

where m is a proportionality constant between the bulk resistivity and the junction resistivity. The proportionality constant is assumed to be based upon the number of conducting bonds in the nanocomposite as well as the overall geometry of the nano-circuitry. Because each sample has the same volume fraction of NiNs, and the filler was homogenously mixed in each sample, it is assumed that the proportionality constant, m, is consistent between different polymers.

Using Equation 3-2 and Equation 3-12 an empirical value for m can be calculated for each material, based upon measured bulk resistivity. A value of m = 0.531 for Sylgard was calculated and applied to Polycrylic and CARC (the only other two polymers with complete data) to calculate the bulk resistivity. The percent error for the calculated bulk resistivity was 5.17 % and 271.86 % for Polycrylic and CARC, respectively. Despite the broad range of barrier heights (0.28 eV and 0.9 eV) and junction distances (3.28 nm and 1.56 nm) for Sylgard and Polycrylic, respectively, this model accurately predicts the bulk resistivity of Polycrylic. This suggests that this model may be functioning well. However, the CARC results highlight that even if the model is functioning well at the nano-junction level, there are other factors that need to be considered that are not currently addressed. One such factor that is suspect is the geometrical connectivity of the internal electrical circuit, which could change from one polymer to another due to different viscosity and processing conditions, which is not adequately captured by the simple linear model.

3.4 Conclusions

Methods have been improved upon to calculate the barrier height of polymers using nanoindentation. Further testing and sampling will continue to improve upon the measured results. The barrier height for three polymers using the improved nanoindenting method were calculated and used to determine the junction distance which yielded results in the 1-2 nm range which correlates well to previous research.

In previous research dielectric spectroscopy has been used in nanocomposites consisting of carbon black and carbon nanotube conductive fillers to measure the junction distance. In this research it has been determined that the same methods can be used to determine the junction distance in nickel nanostrand nanocomposites. The junction distance can be used to determine

the adsorbed layer thickness of polymers on nickel nanostrands. This adsorbed layer thickness has been found to correlate well to the resistivity in the neat polymer.

Also, with a known resistivity of a nanocomposite above the percolation limit and the barrier height the junction distance can be approximated. Using the measured resistivity of the nanocomposite the junction distance was calculated and compared to the junction distance measured using dielectric spectroscopy. R esults were similar suggesting that dielectric spectroscopy is a valid method for junction distance calculation.

With knowledge of the barrier height and the junction distance in a polymer the resistivity of a nanojunction can be determined. U sing the nanojunction resistivity and a proportionality constant the resistivity of a bulk nanocomposite can be determined. This method yielded excellent results for two fully analyzed polymers with widely different barrier height and junction gap properties (Sylgard and Polycrylic); but the third fully characterized polymer did not produce such a low error, indicating a different nano-filler circuitry resulting from the processing route, or some other missing factor in the framework.

With these options for measuring intrinsic material properties the tools are now in place for determining the physical constants necessary for supplying to a quantum tunneling/percolation model of conductive nanocomposites.

REFERENCES

1. Gibson, R.F., *Principles of Composite Materials Mechanics*. 2 ed. 2007, Boca Raton: CRC Press.

2. Callister, W.D., *Materials Science and Engineering: An Introduction*. 7 ed. 2007: Wiley. 832.

3. Roberts, T. *The Carbon Fibre Industry Worldwide 2008-2014*. 2009 [cited 2011 Sept. 30]; Available from: http://www.netcomposites.com/netcommerce_features.asp?1678.

4. Strong, A.B., *Fundamentals of Composites Manufacturing: Materials, Methods, and Applications*. 2 ed. 2008, Dearborn: Society of Manufacturing Engineers. 620.

5. McMahon, C., *Structural Materials*. 2006: Merion Books. 470.

6. Johnson, T., *Strain Monitoring of Carbon Fiber Composite with Embedded Nickel Nanocomposite Strain Gage*, in *Mechanical Engineering*. 2011, Brigham Young University: Provo. p. 82.

7. Manias, E., *Nanocomposites: Stiffer by design.* Nat Mater, 2007. **6**(1): p. 9-11.

8. Al-Saleh, M.H. and U. Sundararaj, *A review of vapor grown carbon nanofiber/polymer conductive composites.* Carbon, 2009. **47**(1): p. 2-22.

9. Ma, H.M. and X.L. Gao, *A three-dimensional Monte Carlo model for electrically conductive polymer matrix composites filled with curved fibers.* Polymer, 2008. **49**(19): p. 4230-4238.

10. Grossiord, N., et al., *High-Conductivity Polymer Nanocomposites Obtained by Tailoring the Characteristics of Carbon Nanotube Fillers.* Advanced Functional Materials, 2008. **18**(20): p. 3226-3234.

11. Li, N., et al., *Electromagnetic Interference (EMI) Shielding of Single-Walled Carbon Nanotube Epoxy Composites.* Nano Letters, 2006. **6**(6): p. 1141-1145.

12. Lalli, J.H., et al. *Commercial applications of Metal Rubber*. 2005: SPIE.

13. Johnson, O., et al., *Multiscale Model for the Extreme Piezoresistivity in Silicone/Nickel Nanostrand Nanocomposites.* Metallurgical and Materials Transactions A, 2011. **42**(13): p. 3898-3906.

14. Park, J.-M., et al., *Inherent sensing and interfacial evaluation of carbon nanofiber and nanotube/epoxy composites using electrical resistance measurement and micromechanical technique.* Composites Part B: Engineering, 2007. **38**(7–8): p. 847-861.

15. Park, J.-M., et al., *Self-sensing and dispersive evaluation of single carbon fiber/carbon nanotube (CNT)-epoxy composites using electro-micromechanical technique and nondestructive acoustic emission.* Composites Part B: Engineering, 2008. **39**(7-8): p. 1170-1182.

16. Stübler, N., J. Fritzsche, and M. Klüppel, *Mechanical and electrical analysis of carbon black networking in elastomers under strain.* Polymer Engineering & Science, 2011. **51**(6): p. 1206-1217.

17. Johnson, T.M., D.T. Fullwood, and G. Hansen, *Strain monitoring of carbon fiber composite via embedded nickel nano-particles.* Composites Part B: Engineering, (0).

18. Johnson, O.K., et al., *The colossal piezoresistive effect in nickel nanastrand polymer composites and a quantum tunneling model.* Computers, Materials & Continua, 2010. **15**(2): p. 24.

19. Tuttle, M. and H. Brinson, *Resistance-foil strain-gage technology as applied to composite materials.* Experimental Mechanics, 1984. **24**(1): p. 54-65.

20. Hill, K.O. and G. Meltz, *Fiber Bragg grating technology fundamentals and overview.* Lightwave Technology, Journal of, 1997. **15**(8): p. 1263-1276.

21. Hu, N., et al., *Tunneling effect in a polymer/carbon nanotube nanocomposite strain sensor.* Acta Materialia, 2008. **56**(13): p. 2929-2936.

22. Angelidis, N., C.Y. Wei, and P.E. Irving, *The electrical resistance response of continuous carbon fibre composite laminates to mechanical strain.* Composites Part A: Applied Science and Manufacturing, 2004. **35**(10): p. 1135-1147.

23. Wang, X., X. Fu, and D.D.L. Chung, *Strain sensing using carbon fiber.* Journal of Materials Research, 1999. **14**(3): p. 12.

24. Xiaojun, W. and D.D.L. Chung, *Continuous carbon fibre epoxy-matrix composite as a sensor of its own strain.* Smart Materials and Structures, 1996. **5**(6): p. 796.

25. Johnson, O.K., et al. *Multi-scale model for the extreme piezoresistivity in silicone/nickel nanostrand nanocomposites*. in *TMS Annual Meeting and Exhibition*. 2010. Seattle, WA.

26. Hansen, N., et al., *Investigation of Electrically Conductive Structural Adhesives using Nickel Nanostrands.* Journal of Adhesion Science and Technology, 2011. **25**(19): p. 2659-2670.

27. Composites, C. *Nickel Chemical Vapor Deposition (CVD) Coated Fibers*. 2011 5/4/2012]; Available from: http://www.conductivecomposites.com/fibers.html.

28. Hansen, G., *The Roles of Nanostrands and Nickel Coated Fibers in Electrically Conductive Composites Design*, in *37th ISTC*. 2005, SAMPE: Seattle, WA.

29. Yoshimoto, S., et al., *Four-Point Probe Resistance Measurements Using PtIr-Coated Carbon Nanotube Tips.* Nano Letters, 2007. **7**(4): p. 956-959.

30. Sirohi, J. and I. Chopra, *Fundamental Understanding of Piezoelectric Strain Sensors.* Journal of Intelligent Material Systems and Structures, 2000. **11**(4): p. 246-257.

31. Johnson, O.K., et al., *Optimization of nickel nanocomposite for large strain sensing applications.* Sensors and Actuators A: Physical, 2011. **166**(1): p. 40-47.

32. Ambrosetti, G., et al., *Solution of the tunneling-percolation problem in the nanocomposite regime.* Physical Review B, 2010. **81**(15): p. 155434.

33. Fritzsche, J., H. Lorenz, and M. Klüppel, *CNT Based Elastomer-Hybrid-Nanocomposites with Promising Mechanical and Electrical Properties.* Macromolecular Materials and Engineering, 2009. **294**(9): p. 551-560.

34. Litvinov, V.M. and P.A.M. Steeman, *EPDM−Carbon Black Interactions and the Reinforcement Mechanisms, As Studied by Low-Resolution 1H NMR.* Macromolecules, 1999. **32**(25): p. 8476-8490.

35. Litvinov, V.M., et al., *Rubber–Filler Interactions and Network Structure in Relation to Stress–Strain Behavior of Vulcanized, Carbon Black Filled EPDM.* Macromolecules, 2011. **44**(12): p. 4887-4900.

36. Reetz, M.T., et al., *Visualization of Surfactants on Nanostructured Palladium Clusters by a Combination of STM and High-Resolution TEM.* Science, 1995. **267**(5196): p. 367-369.

37. Tadd, E., et al., *Adsorption and Polymer Film Formation on Metal Nanoclusters.* Macromolecules, 2003. **36**(17): p. 6497-6502.

38. Pliskin, I. and N. Tokita, *Bound rubber in elastomers: Analysis of elastomer-filler interaction and its effect on viscosity and modulus of composite systems.* Journal of Applied Polymer Science, 1972. **16**(2): p. 473-492.

39. Klüppel, M., *The Role of Disorder in Filler Reinforcement of Elastomers on Various Length Scales Filler-Reinforced Elastomers/Sanning Force Microscopy*. 2003, Springer Berlin / Heidelberg. p. 1-86.

40. Meier, J.G. and M. Klüppel, *Carbon Black Networking in Elastomers Monitored by Dynamic Mechanical and Dielectric Spectroscopy.* Macromolecular Materials and Engineering, 2008. **293**(1): p. 12-38.

41. Meier, J.G., J.W. Mani, and M. Klüppel, *Analysis of carbon black networking in elastomers by dielectric spectroscopy.* Physical Review B, 2007. **75**(5): p. 054202.

42. Woo, D.H., et al., *Current–distance–voltage characteristics of electron tunneling through an electrochemical STM junction.* Surface Science, 2007. **601**(6): p. 1554-1559.

43. Nam-Suk, L., et al. *Study on tunneling current through barrier height using scanning tunneling microscopy*. in *Nanotechnology Materials and Devices Conference, 2006. NMDC 2006. IEEE*. 2006.

44. Yamada, Y., et al., *Local Tunneling Barrier Height Measurement on Au(111).* Japanese Journal of Applied Physics, 2003. **42**(Part 1, No. 7B): p. 4898 - 4900.

45. Yeager, J.D., et al., *Examining chemical structure at the interface between a polymer binder and a pharmaceutical crystal with neutron reflectometry.* Polymer, 2011. **52**(17): p. 3762-3768.

46. Theeten, J.B. and D.E. Aspnes, *Ellipsometry in Thin Film Analysis.* Annual Review of Materials Science, 1981. **11**(1): p. 97-122.

47. Johnson, O., et al., *Characterization of Electrical Properties of Polymers for Conductive Nano-Composites*, in *Society for the Advancement of Material and Process Engineering*. 2011: Long Beach, CA. p. 9.

48. Ahn, J. and M. Pyo, *Comparison of STM Barrier Heights on HOPG in Air and Water.* Bulletin of the Korean Chemical Society, 2000. **21**(6): p. 3.

49. Kawamoto, H., *Carbon Black - Polymer Composites, The Physics of Electrically Conducting Composites*, ed. E.K. Sichel. 1982, New York: Marcel Dekker Inc. 212.

50. Jager, K.-M., et al., *Electron transport and ac electrical properties of carbon black polymer composites.* Journal of Physics D: Applied Physics, 2001. **34**(17): p. 8.

51. Medalia, A.I., *Electrical conduction in carbon black composites.* Rubber Chem. Technol., 1986. **59**(3): p. 23.

52. Packard, H. *Dielectric Constant Measurement of Solid Materials*. [cited 2011; Available from: www.hpmemory.org/an/pdf/an_380-1.pdf.

53. Cole, K.S. and R.H. Cole, *Dispersion and A bsorption in Dielectrics I. Alternating Current Characteristics.* The Journal of Chemical Physics, 1941. **9**(4): p. 341-351.

54. Sheng, P., E.K. Sichel, and J.I. Gittleman, *Fluctuation-Induced Tunneling Conduction in Carbon-Polyvinylchloride Composites.* Physical Review Letters, 1978. **40**(18): p. 1197-1200.

55. Fritzsche, J. and M. Klüppel, *Structural dynamics and i nterfacial properties of filler-reinforced elastomers.* Journal of Physics: Condensed Matter, 2011. **23**(3): p. 035104.

56. Corning, D. *Sylgard 184 Si licone Elastomer Kit*. 2012; Available from: http://www.dowcorning.com/applications/search/default.aspx?r=131en.

57. Hansen, N., et al., *Investigation and correlation of percolation behaviors and phy sical properties in electrically conductive nickel nanostrand polymer composites.* To be published, 2012.